



Identifying where and when urban renewal occurs: a continuous change detection-based framework using two decades' worth of Landsat data

Chong Liu^{a,b}, Qi Zhang^c, Huabing Huang^{a,b}, Hanzeyu Xu^{d,e,f} and Xiao Cheng^{a,b}

^aSchool of Geospatial Engineering and Science, Sun Yat-sen University, Guangzhou, People's Republic of China; ^bKey Laboratory of Comprehensive Observation of Polar Environment (Sun Yat-sen University), Ministry of Education, Zhuhai, People's Republic of China; ^cDepartment of Geography and Environment, University of North Carolina at Chapel Hill, Chapel Hill, NC, USA; ^dJiangsu Key Laboratory of Crop Genetics and Physiology/Jiangsu Key Laboratory of Crop Cultivation and Physiology, Agricultural College of Yangzhou University, Yangzhou, People's Republic of China; ^eJiangsu Co-Innovation Center for Modern Production Technology of Grain Crops, Yangzhou University, Yangzhou, People's Republic of China; ^fResearch Institute of Smart Agriculture, Yangzhou University, Yangzhou, People's Republic of China

ABSTRACT

Urban renewal plays a central role in enhancing city liveability by rebuilding outdated structures into productive and vibrant spaces. While satellite remote sensing enables physical characterization of urban environments, identifying the precise location and timing of renewal remains challenging. Here we developed a 30 m city-scale urban renewal mapping framework with the use of dense Landsat time-series information. By leveraging the Continuous Change Detection and Classification (CCDC) algorithm, we designed a decision tree model to identify pixels experiencing urban renewal and utilized the temporal contextual knowledge to estimate temporal metrics, including start time (ST), end time (ET), and duration (DUR). Experimental results in Beijing city confirmed the feasibility of the framework, achieving spatial and temporal accuracies of 82.36% and 71.39~86.60%, respectively. Our mapping results revealed that the total area of urban renewal within the study area reached 340 ± 55 km² from 1999 to 2019, distributed unevenly along the urban-rural gradient. We also identified the dominance of quick demolition and reconstruction implementation accomplished within five years. The framework provides a new paradigm for continuously monitoring city development from the perspective of urban renewal, thus supporting the improvement of urban land planning and management.

ARTICLE HISTORY

Received 26 November 2024
Accepted 16 May 2025

KEYWORDS

Urban renewal; land cover; segments classification; change detection; CCDC

1. Introduction

Urban areas are an idiosyncrasy of human footprint on the Earth's terrestrial surface (Acuto, Parnell, and Seto 2018; Liu et al. 2019; Gong et al. 2020). For the first time in

CONTACT Xiao Cheng chengxiao9@mail.sysu.edu.cn School of Geospatial Engineering and Science, Sun Yat-sen University, Guangzhou, 510275, People's Republic of China

© 2025 The Author(s). Published by Informa UK Limited, trading as Taylor & Francis Group
This is an Open Access article distributed under the terms of the Creative Commons Attribution-NonCommercial License (<http://creativecommons.org/licenses/by-nc/4.0/>), which permits unrestricted non-commercial use, distribution, and reproduction in any medium, provided the original work is properly cited. The terms on which this article has been published allow the posting of the Accepted Manuscript in a repository by the author(s) or with their consent.

history, more than 50% of global population is now living in cities and towns, a percentage that is expected to approach 70% by 2050 (UN 2017). Moreover, urban areas have profound socio-economic and environmental effects, contributing approximately 80% of world's gross domestic product (GDP) (Zhou et al. 2022), generating 70% of global waste (Zhu et al. 2019), and accounting for 75% of greenhouse gas emissions from worldwide energy use (Solecki, Seto, and Marcotullio 2013; Solecki, Seto, and Marcotullio 2013). Underpinning these socioeconomic activities are unprecedented waves of urbanization and substantial increases in natural resource consumption, which have given rise to critical challenges, including environmental degradation (Grimm et al. 2008; Zhang et al. 2022), slum growth (Reba and Seto 2020), public health issues (Gong et al. 2012), and infrastructure inequality (Zhou et al. 2022; Che et al. 2024). Therefore, the world requires more scientific knowledge than ever to achieve sustainable development from an urban perspective (Seto, Güneralp, and Hutyrá 2012).

In the past few decades, global urbanization was primarily characterized by the expansion of built-up areas (Liu, Huang, et al. 2020). However, with socio-economic development and limited land reserves, the ongoing urbanization process has been gradually shifted from the phase of outward sprawl to the stage of improvement within existing urban regions, especially in developing countries under economic boost such as China and India (Manupati, Ramkumar, and Samanta 2018; Frolking et al. 2024). Urban renewal (also termed as urban regeneration/redevelopment) is an essential strategy for policymakers to revitalize urban spaces that are outdated and no longer conducive to contemporary social living (Liu, Wei, et al. 2020). By demolishing unsuitable residential buildings and municipal facilities, new constructions can be promoted to boost land values and enhance environmental quality (Zhang, Zhang, and Lin 2014). At the city level, urban renewal is usually associated with land surface morphology change (Zhao, Chen, et al. 2023), and therefore plays a critical role in regulating energy fluxes (Ahmadian et al. 2021; Bansal and Quan 2022). Despite its economic and ecological importance, the spatiotemporal pattern of urban renewal has been rarely quantified across scales, and most of our current understanding of urban renewal is still generated using national/city's statistics (Zhang, Zhang, and Wu 2021) or based on field investigations (Hashemi-Parast, Yamazaki, and Liu 2017), both of which suffer from sparse spatial representative and inconsistent accuracy (Zhao, Xia, and Li 2023).

The emergence of Earth-observing satellites has significantly enhanced our capacity to understand urbanization processes, with remote sensing techniques being widely utilized to characterize land cover and land use changes (LCLUC) associated with urban renewal. For instance, Yue et al. (2006) employed sub-pixel classification of satellite imagery from two distinct periods to assess urban functional dynamics in Shanghai, China. This approach was further advanced in a more recent study by Qiao et al. (2020), which incorporated multi-source remote sensing data. Although these post-classification analyses are straightforward and capable of identifying where urban renewal activities are located, they do not address temporal concerns such as when do urban renewal activities start/end and how long do they last. These challenges highlight the necessity of using denser time series remote sensing data to understand the complete timeline of urban renewal, including demolition and reconstruction (Ni et al. 2023; Wang et al. 2023). The unrestricted access to the Landsat dataset since 2008 has facilitated unprecedented opportunities for advancing the monitoring and analysis of land surface condition

(Wulder et al. 2022). With the pixel size of 30 m and the revisit cycle of 16 days, time series Landsat observations enable the monitoring of comprehensive urbanization information including building age (Hu et al. 2024; Zhuo et al. 2024), city regreening (Zhang, Brandt, et al. 2024), and urban morphology changes (Wang et al. 2023). However, these urban environment monitoring approaches are not specifically tailored for urban renewal, and most of them bear with limited temporal frequency and flexibility, making them less applicable in areas undergoing quick demolition and reconstruction that typically accomplished within 2~3 years.

The enhanced accessibility of remotely sensed imagery, coupled with the growing availability of cloud computing resources and platforms like Google Earth Engine (GEE hereafter) (Gorelick et al. 2017), has substantially broadened the community of users engaged in processing and analyzing satellite observation time series (Potapov et al. 2020). Based on this premise, recent years have witnessed the development of specialized temporal segmentation algorithms for fine-grained land surface change monitoring, such as LandTrendr (Landsat-based detection of Trends in Disturbance and Recovery) (Kennedy, Yang, and Cohen 2010; Kennedy et al. 2015), BFAST (Break detection For Additive Season and Trend) (Verbesselt, Zeileis, and Herold 2012), CCDC (Continuous Change Detection and Classification) (Zhu et al. 2015), VCT (Vegetation Change Tracker) (Huang et al. 2010) and C2C (Composite2Change) (Hermosilla et al. 2016). Among them, LandTrendr, VCT, and C2C are trajectory-based change detection algorithms that utilize annual stacks of satellite imagery, relying on the availability of cloud-free composites for accurate temporal analysis. Therefore, these methods are primarily useful for natural ecosystems and may not perform as well in non-vegetated or highly heterogeneous landscapes (Cohen et al. 2018). In contrast, CCDC leverages all available imagery to generate predicted values, enabling change detection at flexible temporal scales and supporting near-real-time monitoring capabilities. Moreover, CCDC stands out for its ability to continuously monitor changes while simultaneously classifying land cover, making it a powerful tool for comprehensive land cover applications including LCLUC (Wang et al. 2020; Xian et al. 2022), forest disturbance (Zhang et al. 2022), and plantation abandonment/regrowth (Xu et al. 2021). Although exhibiting great potential for land surface monitoring, CCDC has been seldomly used to study large area urban renewal processes, which is due primarily to the fact that running CCDC requires substantial computational resources, as it involves per-pixel, repeated model fitting on extensive time series imagery. The high computation and storage costs have unnecessarily restricted its practical application, especially in urban areas where enhanced land surface monitoring knowledge is critically required (Hu et al. 2024). This predicament has been alleviated by the implementation of the CCDC algorithm on GEE platform (Arévalo et al. 2020). More recently, Gorelick et al. (2023) used two decades' Landsat archives to implement the change detection component of CCDC (CCD hereafter) at a global scale, and ported the resulting segments product into Earth Engine Data Catalog, which further facilitates fine resolution (compared with coarse satellite sensors such as MODIS and AVHRR) and large area land surface dynamics applications.

Based on the complete Landsat achieve over a 20-year period (1999~2019), the objective of this study is to establish a spatiotemporally continuous framework to monitor urban renewal dynamics at a fine resolution (30 m) city scale. Here, urban renewal refers to the complete process of removing old built-up areas and reconstructing new ones (Zheng, Shen, and Wang 2014). We utilized the CCDC algorithm to identify all

land cover change(s), which were adopted for estimating per-pixel existence of urban renewal based on a decision tree model. Temporal contextual information was then employed to derive key temporal metrics associated with urban renewal processes. We aim, by identifying where and when urban renewal activities occur, to advance our understanding of urban environmental change, which will benefit the ongoing efforts on sustainable development goals by public/governmental sectors.

2. Materials and methods

2.1. Study area

Our study area is Beijing city ($39^{\circ}26' \sim 41^{\circ}03' \text{N}$, $115^{\circ}25' \sim 117^{\circ}30' \text{E}$) (Figure 1(a)), which is located at the northern tip of the North China Plain with a population of 21.89 million (BMBS 2020). The topography of Beijing is highly diverse, ranging from flat plains in the southeastern part, to mountains along its western and northern borders. As the country's capital, Beijing exemplifies many other big cities in China that suffer from social, environmental, and infrastructural problems due to rapid urbanization and population growth. To combat these challenges and pursue sustainable development, considerable efforts have been made on the reconstruction of existing built-up areas during the past decades in Beijing (Ni et al. 2023), providing a valuable opportunity for us to assess the proposed framework of urban renewal information extraction.

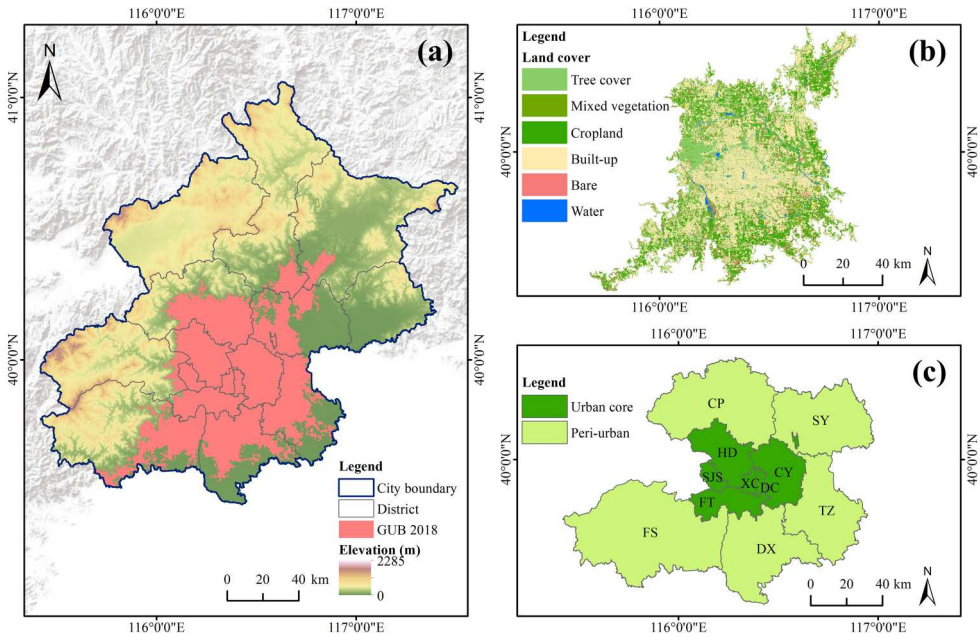


Figure 1. The study area: Beijing city. (a) Overview of the study area (DEM source: Copernicus DEM GLO-30). (b) Zoom-in view of Beijing's urban space defined by the global urban boundary dataset (GUB) in 2018. The land cover distribution is derived from the ESA WorldCover 2020 product. The mixed vegetation class encompasses grassland, shrubland, and herbaceous wetland. (c) Eleven Administrative districts (CP, CY, DX, DC, FS, FT, HD, SJS, SY, TZ, and XC) involved in this study. The district abbreviations are given in Section 2.1 of the main text.

For the spatial extent, we focus on the urban core and its surrounding area of Beijing, defined by the global urban boundary dataset in 2018 (Li, Gong, et al. 2020) (see Section 2.2.2). This is because most urban renewal occurred within this area. Although urban renewal also exists in places outside the delimited boundary, they are rather scattered in relatively small scales (Wang et al. 2023) and hence negligible for testing the algorithm framework in this study. After spatial filtering, our study area covers a total of 5,715 km² (34.83% of the total land surface area of Beijing) and encompasses multiple land cover types, including built-up, cropland, forest, mixed vegetation, water, and bare soil. (Figure 1(b)). Of the eleven administrative districts involved in this study (Figure 1(c)), six (Chaoyang (CY), Dongcheng (DC), Fengtai (FT), Haidian (HD), Shijingshan (SJS) and Xicheng (XC)) are situated in the center of Beijing and are recognized as the urban core, whereas the remaining five (Changping (CP), Daxing (DX), Fangshan (FS), Shunyi (SY) and Tongzhou (TZ)) are regarded as peri-urban regions.

2.2. Datasets

2.2.1. Global Landsat-based CCD segments

Gorelick et al. (2023) implemented CCD at the planetary scale (i.e. all landmasses between 60°S and 85°N) using full daytime Landsat archives from 1999 to 2019. Among available Landsat products, only the category of Collection 1 Tier 1 imagery was used because it has high geo-registration precision, well-characterized radiometry and is inter-calibrated across different Landsat instruments (<https://www.usgs.gov/landsat-missions/landsat-collection-1>), all of which are essential features for robust time series analysis (Liu et al. 2019; Liu, Zhang, et al. 2020). Different from previous attempts for local academic uses, this new implementation aims to enable worldwide, dense Landsat time series processing and information extraction. For this purpose, a pre-computed global CCD product was generated using the default parameters in version 12.30 of the MATLAB implementation (Gorelick et al. 2023) and subsequently integrated into the GEE cloud environment as a standalone image collection asset. As Figure 2 illustrates, this CCD product identifies statistical breakpoints within Landsat time series data and further models surface reflectance over time. Two adjacent breaks jointly determine a time segment that is assumed to depict stable land cover with distinct spectral signatures. Each pixel thus contains a sequence of one or more of these time segments. The outputs of each time segment have a pixel size of 30 m, and contain four groups of geospatial parameter layers including: (1) the number of Landsat observations (one layer); (2) the start, end, and breakpoint dates (three layers); (3) the per-band harmonic coefficients (56 layers), modeled root mean square error (RMSE) (seven layers), and magnitude of the detected breakpoint (seven layers); (4) the pseudo-probability of the detected breakpoint being true (one layers). Readers can refer to (Gorelick et al. 2023) for additional details of this global CCD product. In our study, we filtered the CCD image collection by the extent of the study area, and used the ‘Suite of Tools for CCDC’ (Arévalo et al. 2020) in GEE to visualize and manipulate CCD outputs.

2.2.2. Auxiliary data

In addition to the Landsat-based CCD segments, three auxiliary data were further used in this study. The first is the global urban boundary (GUB) dataset (Li, Gong, et al. 2020),

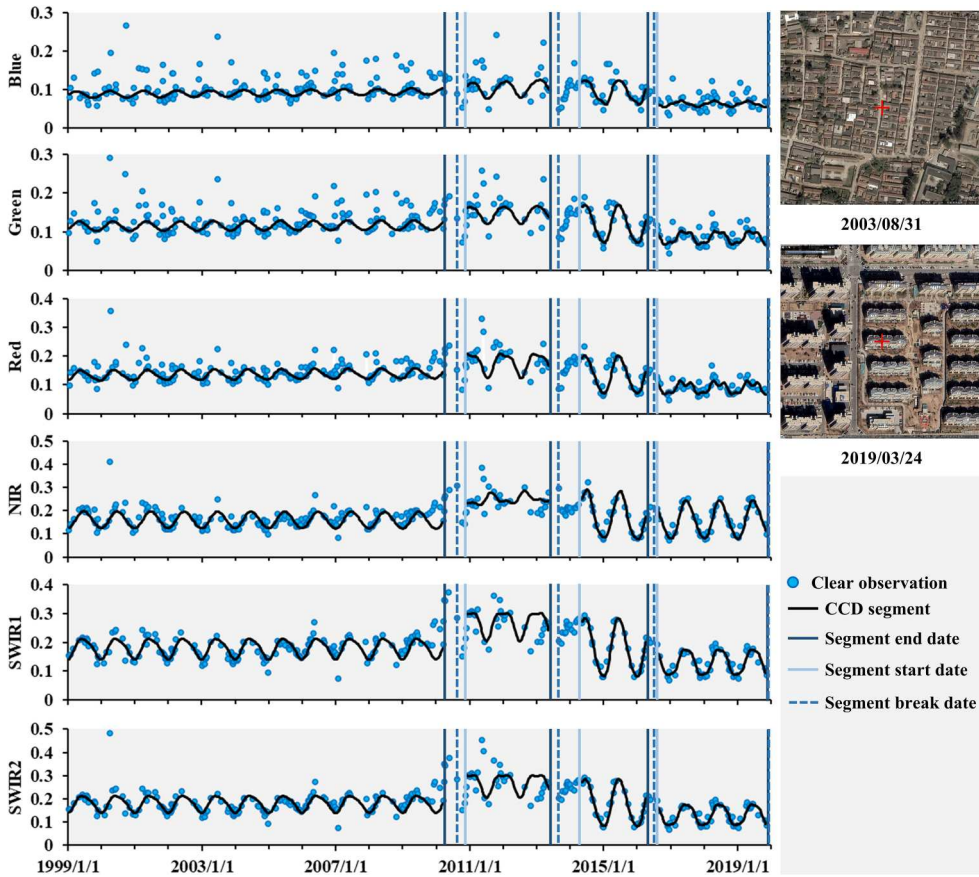


Figure 2. CCD land surface change detection and segmentation for an urban renewal pixel. Blue dots represent clear Landsat observations. The black curve is the model fit including four segments separated by detected breakpoints. Segment end date, start date, and break date are labeled by dark blue solid line, light blue solid line, and dashed line, respectively. The high resolution images (derived from Google Earth) display land surface conditions in 2003 (before urban renewal) and 2019 (after urban renewal), respectively.

which was created from the global artificial impervious area (GAIA) product (Gong et al. 2020) and provides worldwide polygon features for urban/non-urban separation. Note that the GUB dataset contains seven epochs (1990, 1995, 2000, 2005, 2010, 2015, 2018), from which the latest result (GUB 2018) was used to delimit the urban extent of Beijing. The second auxiliary dataset is ESA WorldCover (Zanaga et al. 2021). This dataset offers global-scale 30 m land cover information based on a 11-category classification scheme. Here only the WorldCover product for the nominal year of 2020 (WorldCover 2020 hereafter) was selected to reduce uncertainty from temporal disagreement. We further adjusted the original classification system of WorldCover 2020 by merging mixed vegetation types, including grassland, shrubland, and herbaceous wetland (Xu et al. 2024). The third auxiliary dataset is the Copernicus Digital Elevation Model dataset at the 30 m spatial resolution (i.e. GLO-30 DEM, <https://spacedata.copernicus.eu/collections/copernicus-digital-elevation-model>), from which we obtained three

topographic variables, which were elevation, slope and aspect. These variables served as additional image features for CCD segments classification.

2.3. Methods

2.3.1. Overview of the proposed framework

From the perspective of LCLUC, urban renewal is a complex process that displays sequential changes from built-up land to urban vacant land (e.g. bare soil with grass or water), and then back to built-up land again. Based on this premise, we developed an algorithm framework to estimate the existence of urban renewal and characterized its spatiotemporal patterns across the study area, using the Landsat-based CCD segments product and other auxiliary data with the pixel size of 30 m. The framework was applied for pixel-level analysis, so the pixel-based consistency across time can be guaranteed. Figure 3 illustrates the flow chart of the developed framework, which includes three major modules: (1) CCD segments classification, (2) urban renewal information extraction, (3) evaluation and analysis. In the first module, we generated a training sample set that was consistent throughout the study years and used it to determine the land cover type of each time segment by performing a machine learning-based classification procedure. With the classified segments dataset, the second module was conducted to extract per-pixel urban renewal information. To achieve this goal, we designed a decision tree model to identify pixels that experienced urban renewal and leveraged the CCD-detected, temporal contextual information to estimate three metrics of urban renewal, including its start time (ST), end time (ET), and duration (DUR). Finally, we evaluated

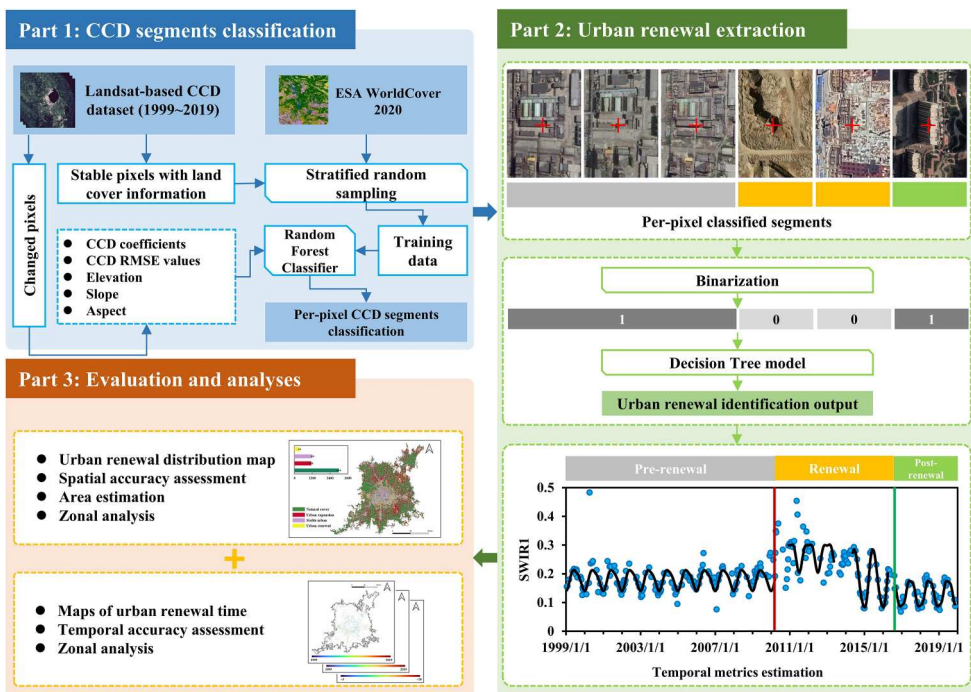


Figure 3. Flow chart of the developed framework for urban renewal information extraction.

the generated urban renewal maps and analyzed their spatiotemporal patterns. The proposed framework was implemented on the GEE platform.

2.3.2. CCD segments classification

We constructed the training data set before implementing the time segments classification. Traditionally, training data were collected by field investigation or interpreted from high resolution imagery, both of which can be labor intensive. To address this issue, some studies migrated training data from existing land cover products or sample libraries for their respective uses (Gray and Song 2013; Huang et al. 2020). Following these endeavors, we developed a method that generated consistent training data with the combined use of the Landsat-based CCD segments product and WorldCover 2020. The first step of the method was to identify all available stable pixels within the study area. Here, 'stable' means no abrupt land surface change is detected by CCD, and therefore a consistent land cover type can be assumed. Once stable pixels were determined, their associated land cover classes were labeled by WorldCover 2020, and these labeled stable pixels were regarded as the classification reference. To minimize the impact of misclassification within the WorldCover 2020 map, the identified stable pixels were further refined by applying a class-specific erode filter with a 3×3 pixel kernel (Zhang, Zhao, et al. 2024).

While the pool of stable pixels contained millions of potential training pixels, land cover class size and distribution were highly unbalanced. Therefore, we implemented a stratified random sampling strategy to optimize the selection of the training data. The six strata in the training sampling design were tree cover, mixed vegetation, cropland, built-up, bare land, and water (i.e. all modified WorldCover 2020 classes in the study area). Following the suggestion of Zhu et al. (2016), an initial training sample size of 20,000 was used in this study. The sample size of each stratum was determined according to its mapped area by WorldCover 2020. It is important to note that such a proportional sample allocation may result in extremely large or small sample sizes for some strata (Zhang, Zhao, et al. 2024). To achieve a better sample balance, we enlarged the sample size to reach the minimum if a stratum had fewer training pixels than the minimum required. In contrast, we reduced the sample count to meet the maximum if a stratum involved more training pixels than the maximum allowed. The minimum and maximum training pixel number limits per stratum were 600 and 8,000, respectively (Zhu et al. 2016; Zhang, Zhao, et al. 2024). After visually verifying and removing incorrect pixels, the final training dataset contains 19,923 stable pixels, including 4,654, 702, 5,084, 7,961, 925, and 597 randomly selected pixels for tree cover, mixed vegetation, cropland, built-up, bare land, and water, respectively.

Based on the generated training sample dataset, we implemented the classification component of CCDC for all changed pixels in the study area. Unlike conventional approaches that directly classify the satellite image, we used the segment as the basic classification unit. By predicting each segment's land cover type, a classified sequence throughout the study period can be generated at the pixel level for urban renewal information extraction. In this study, the classifier feature inputs came from three variable groups. The first group consists of harmonic model coefficients from Landsat surface reflectance and thermal bands, representing spectral patterns of different land cover types at the temporal domain. The second variable group was the per-band model

RMSE value that quantifies the agreement level between the CCD model estimation and the actual Landsat observation. We also included three topographic variables (elevation, slope and aspect) from the GLO-30 DEM dataset as the third variable group. The feature extraction procedure resulted in a total of 66 variables as inputs to the Random Forest Classifier (RFC) (Breiman 2001). This machine learning method was used as the supervised classifier because it can handle high dimensional feature spaces and is robust over large areas (Dannenberg, Hakkenberg, and Song 2016; Liu et al. 2019). For the purpose of balancing the classification accuracy and computational cost, we configured RFC to use 300 decision trees (Belgiu and Drăguț 2016; Liu et al. 2021), and determined the number of features for splitting each node as the square root of the total number of input feature variables.

2.3.3. Identification of urban renewal existence

Although the urban renewal process is highly complex, it follows two basic principles at the temporal domain: (1) the land cover class should be built-up at its initial and final states; (2) there should exist land cover change(s) during the study period. Using these principles as priori knowledge, we designed a decision tree model to map the per-pixel existence of urban renewal. Taking a given pixel i as an example, Figure 4 provides a schematic demonstration of the model. First of all, we relabeled the segments classification result to create a binary time series profile, indicating the land cover condition (built-up as 1, others as 0) at each segment. Then, several decision rules were employed to identify pixel i as one of the following four types: natural cover, urban expansion, stable urban, and urban renewal.

- (1) Identifying non-renewal pixel types. If the last segment was labeled as 0 ($Sn_{class} = 0$), pixel i was identified as natural cover. Otherwise, we moved on to the next step by checking the first segment. If it was labeled as 0 (i.e. $S1_{class} = 0$ and $Sn_{class} = 1$), we regarded pixel i as land experiencing urban expansion. Since both urban renewal and stable urban areas exhibit the same land cover classes at the initial and final states (i.e. $S1_{class} = 1$ and $Sn_{class} = 1$), additional steps were carried out for their identification. A distinct characteristic of urban renewal is that it involves land cover change(s), so pixel i was identified as stable urban land if no break was found by CCD ($Chg_{num} = 0$).
- (2) Excluding false alarms. We further considered the impact of ‘false changes’ detected by CCD, which would result in statistical breakpoint(s) but unaltered land cover condition (i.e. false alarms). Given that the urban renewal process, as mentioned in Section 2.3.1, usually includes a vacant land period characterized by bare soil or vegetation (Wang et al. 2023; Zhao, Xia, and Li 2023), It can be expected that at least one segment classified as non-built-up land cover category after demolition and before reconstruction completion. Otherwise, pixel i was assigned to the stable urban type if its CCD time series included multiple breaks ($Chg_{num} > 1$) but all segments were labeled as 1.
- (3) Dealing with a special case. Noted that the aforementioned decision rules are not applicable if pixel i changed only once ($Chg_{num} = 1$) (i.e. two segments and both labeled as 1). To deal with this special case, we adopted a threshold-based approach to separate stable urban and urban renewal types. Time series breakpoints associated

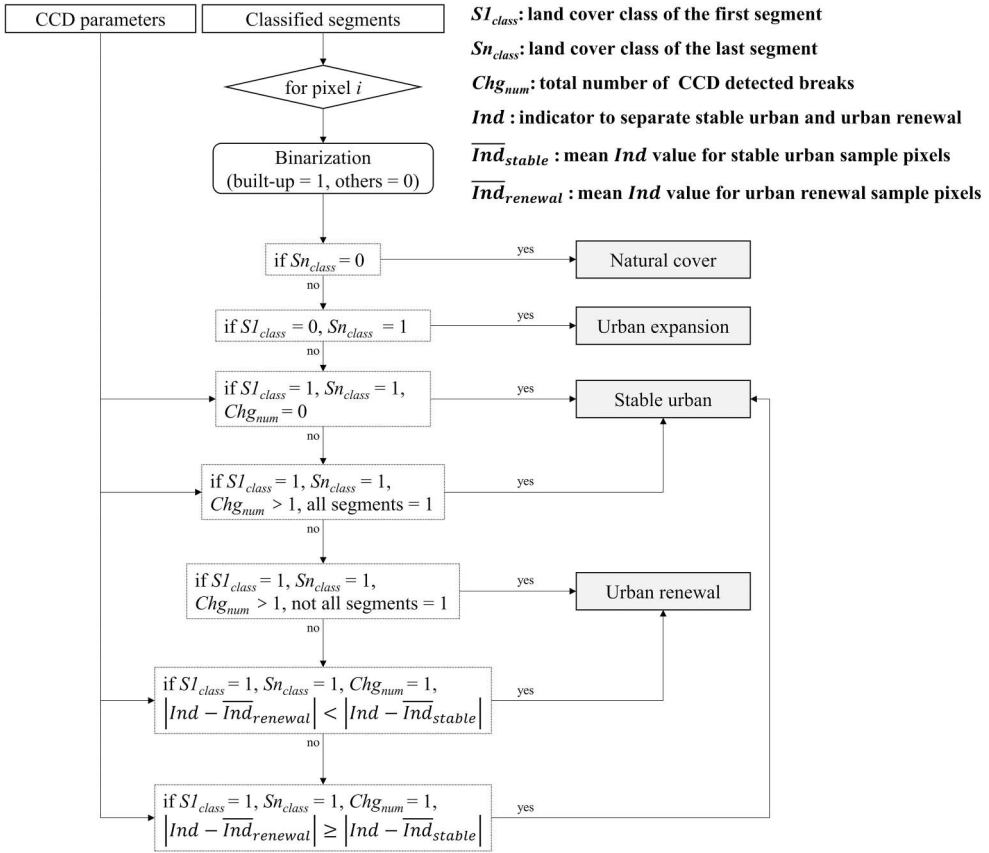


Figure 4. Decision tree model for per-pixel urban renewal identification.

with urban built-up changes often have greater shortwave infrared reflectance change magnitudes than those caused by subtle conditional environment variability (Xian et al. 2022; He et al. 2024), and thus an indicator Ind can be defined as:

$$Ind = abs\left(\frac{SWIR1_magnitude}{S1_SWIR1_rmse}\right) \quad (1)$$

where $SWIR1_magnitude$ represents the CCD detected SWIR1 band change magnitude of the breakpoint (reflectance difference between observation and prediction), $S1_SWIR1_rmse$ is the SWIR1 band derived root mean square error from the first segment model fit, which was used to characterize the relative impact of CCD time series model fitting on the spectral change magnitude. To determine the optimal Ind , 200 sample pixels that experienced one CCD-recorded break were selected, with one half collected from stable urban areas while the other half from the urban renewal areas. Based on the collected sample pixels, we calculated the mean Ind values of stable urban (\overline{Ind}_{stable}) and urban renewal ($\overline{Ind}_{renewal}$),

respectively. For pixel i , the equation of identifying its type can be expressed as:

$$type_i = \begin{cases} \text{urban renewal, } |Ind - \overline{Ind}_{renewal}| < |Ind - \overline{Ind}_{stable}| \\ \text{stable urban, } |Ind - \overline{Ind}_{renewal}| \geq |Ind - \overline{Ind}_{stable}| \end{cases} \quad (2)$$

By applying the decision tree model pixel by pixel, a spatially continuous map of urban renewal distribution can be derived for the study area. We also removed isolated urban renewal patches by setting the minimum map unit (MMU) as 11 connected pixels (Cohen et al. 2018).

2.3.4. Extraction of ST, ET and DUR

Identifying urban renewal existence is important, and knowing when urban renewal activities take place at the pixel level is more valuable. In this study, we used CCD-detected land surface changing information to estimate three temporal metrics of urban renewal including ST, ET and DUR. Among numerous reflectance bands and remote sensing indices, SWIR1 was selected as the spectral indicator because it is sensitive to both demolition and reconstruction changes (Wang et al. 2023; Hu et al. 2024). In general, the land leveling process will result in SWIR1 reflectance increase ($\Delta SWIR1 > 0$). Conversely, the transform from vacant land to new construction is associated with decreased SWIR1 reflectance ($\Delta SWIR1 < 0$). Therefore, the task of pixel level urban renewal temporal metrics estimation can be implemented by finding the first and last CCD breaks exhibiting positive and negative $\Delta SWIR1$, respectively. Figure 5 graphically depicts the determination of three temporal metrics at one example pixel. The built-up area stayed spectrally stable

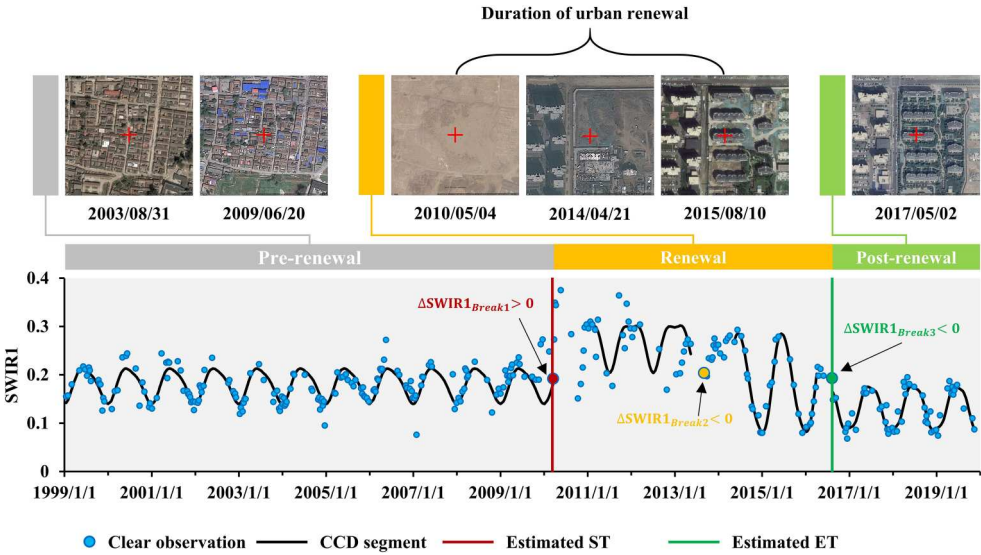


Figure 5. Illustration of estimating three temporal metrics of urban renewal at one example pixel (40° 07'N, 116°38'E). The vertical axis represents the surface reflectance of Landsat SWIR1 band. Blue dots are clear Landsat observations. The vertical lines in red and green colors shows the estimated ST and ET, respectively. $\Delta SWIR1_{Breaki}$ ($i = 1, 2, 3$) indicate SWIR1 reflectance changes for three CCD detected breaks.

during the pre-renewal period (from 1999 to 2009). In 2010, however, demolition was carried out and an abrupt land surface change was identified with positive $\Delta SWIR1$. As a result, ST was determined as the end time of the first segment (2010/03/15). After that, the vacant land was firstly covered by bare soil/vegetation mosaic, and then went through new building construction, resulting in two breaks in 2013 and 2016, respectively. Since both breaks display negative $\Delta SWIR1$, we chose the latter one to separate renewal and post-renewal periods. On this basis, ET was determined as the start time of the last segment (2016/08/08), indicating the completion of urban renewal. Finally, DUR was calculated as the temporal length between ST and ET (6 years 147 days, or 6.40 years). To improve the rationality of the estimated results, we also added a correction procedure if DUR was less than or equal to 0. For this case, ST and ET was simplified as the end and the start time of the first and the last segments, respectively.

2.3.5. Evaluation and analyses

The generated urban renewal maps were evaluated in two aspects: spatial and temporal. For the spatial accuracy assessment, we examined the urban renewal distribution map by designing a stratified random validation sample set. The four strata used were natural cover, urban expansion, stable urban, and urban renewal. For stratified random sampling practices, Olofsson et al. (2014) suggests a validation sample size (n) calculated as:

$$n = \frac{\sum W_i S_i}{S(\hat{\delta})} \quad (3)$$

$$S_i = \sqrt{U_i(1 - U_i)} \quad (4)$$

where W_i , S_i , U_i are the mapped area proportion, the standard deviation, and the expected user's accuracy of stratum i , respectively. $S(\hat{\delta})$ is the standard error of the estimated overall accuracy (OA). By assuming a standard error of 1% for OA and target user's accuracies (0.85, 0.75, 0.85, and 0.75 for natural cover, urban expansion, stable urban, and urban renewal, respectively), **Eq. (3)-(4)** gave a resulting validation sample size of 1,370, which was round to 1,400. We allocated 500 sample units to the urban renewal stratum for reducing the sample-based area estimate uncertainty. The remaining 900 sample units were allocated evenly among the other three strata. The reference category label for each sampled unit was determined by expert interpretation with the support of Landsat Time Series Explorer, a shareable GEE App tool that offers annual stack of image chips around the Landsat pixel of interest, as well as temporal trajectories of spectral bands or indices (<https://jstnbraaten.users.earthengine.app/view/landsat-timeseries-explorer>). Historical images from Google Earth and ESRI living Atlas Wayback (<https://livingatlas.arcgis.com/wayback>) were also used to refine our judgement. If a sample unit was interpreted as urban renewal land, its temporal metrics (ST, ET and DUR) were also recorded at the annual scale. Based on the validation sample set, we calculated four indicators including OA, producer's accuracy (PA), user's accuracy (UA), and F1 score.

From the original 1,400 validation samples used for spatial accuracy assessment, we derived a subset of 388 pixels for temporal domain evaluation through the following rigorous selection: (1) samples must be located in reference-confirmed urban renewal areas, and (2) must have been correctly identified as renewal sites by our algorithm in the spatial domain. This filtered subset underwent annual-scale temporal accuracy

assessment, ensuring that only reliably classified renewal cases were used to evaluate the timing metrics (ST, ET, DUR). We derived the confusion matrix for each of the three estimated metrics (ST, ET, and DUR), and evaluated the agreement between the estimated results and the actual values using OA, systematic error (SE) and root mean squared error (RMSE). Among these indicators, OA was employed to measure the overall precision, while the latter two quantified estimation bias:

$$SE = \frac{1}{n} \sum_{i=1}^n (\hat{t}_i - t_i) \quad (5)$$

$$RMSE = \sqrt{\frac{1}{n} \sum_{i=1}^n (\hat{t}_i - t_i)^2} \quad (6)$$

where \hat{t}_i is the estimated temporal metric result of sample i ; t_i is the reference temporal metric value of sample i ; and n is the total number of sample pixels ($n = 388$). Given the uncertainties within expert interpretation, we implemented two temporal validation schemes: one utilizing the exact year identified from our method, and the other allowing for a one-year tolerance. For the latter one-year tolerance comparison, if the reference year fell within a range of ± 1 year relative to the detected year, it was identified as a fuzzy true detection (Song et al. 2016; Wang et al. 2023).

To better understand the spatiotemporal patterns of urban renewal, we analyzed our mapping results at two different stages. At the first stage, we estimated the total urban renewal area within the entire study domain using the approach proposed by Olofsson et al. (2014), which employs the validation sample to correct bias in mapped areas that is caused by classification errors (Stehman and Foody 2019; Zhang et al. 2022). This approach resulted in the error-adjusted area estimate as well as associated uncertainty (i.e. the 95% confidence interval) for each of the four strata/pixel types: natural cover, urban expansion, stable urban, and urban renewal. At the second stage, per-pixel mapping results were aggregated at the administrative district level to offer spatial representations of where and when urban renewal was most likely to have occurred.

3. Results

3.1. Accuracy assessment

3.1.1. Accuracy of urban renewal existence

Table 1 displays the confusion matrix of 1,400 validation sample units as well as the derived error indicators. In general, we found the spatial mapping result of urban renewal distribution has a high accuracy, with an achieved OA of 82.36% for the entire study area. At the class level, all mapped land cover change types exhibit reasonable performances, with F1 scores ranging from 76.22% to 86.44%. It is worth noting that the urban renewal class displays a higher PA value (92.60%) than UA value (77.60%), indicating a higher probability of commission error within the study area. In contrast, the opposite tendency ($PA < UA$) was observed for other three classes including natural cover, urban expansion, and stable urban. According to the statistics, we further found that most classification errors come from the confusion between urban renewal and stable urban.

Table 1. Accuracy assessment for the urban renewal spatial distribution map using 1,400 validation sample units. UA, PA, F1 and OA are user's accuracy, producer's accuracy, F1 score, and overall accuracy, respectively.

	Reference			
	Natural cover	Urban expansion	Stable urban	Urban renewal
Natural cover	274	14	9	3
Urban expansion	29	249	15	7
Stable urban	6	31	242	21
Urban renewal	25	18	69	388
UA	91.33%	83.00%	80.67%	77.60%
PA	82.04%	79.81%	72.24%	92.60%
F1	86.44%	81.37%	76.22%	84.44%
OA	82.36%			

3.1.2. Accuracy of urban renewal temporal metrics

Figure 6 shows the performance evaluation results of estimated urban renewal temporal metrics using the exact-year and the one-year tolerance strategies, respectively. For each temporal metric, its confusion matrix was constructed based on 388 urban renewal sample units that were correctly classified by our method. Overall, the comparison of reference data and predicted results exhibits a generally reasonable agreement, with most elements concentrated around the 1:1 line. Using the exact-year strategy (Figure 5(a–c)), we found our algorithm framework performed well in calculating ST with OA value of 74.48% and RMSE value of 1.79 years. For ET, we found relatively low OA value of 58.76% and high RMSE value of 2.04 years, which indicates that ET is less accurately predicted than ST is. The precision discrepancy reflects a greater complexity for separating renewal and post-renewal periods. Compared with the demolition of old buildings, urban reconstruction usually takes a longer time and involves multiple LCLUC processes (e.g. vegetation recovery/removal), leading to increased heterogeneity in the spatial and temporal domains (Zhao, Xia, and Li 2023; Hu et al. 2024). Our results also suggest that the estimated ST and ET have opposite SE trends, and their values are both within one year. Since DUR is jointly determined by ST and ET, it is not surprising to find a larger uncertainty reflected by its error indicators (OA = 47.42%, RMSE = 2.63 years). Noted that the validation of urban renewal temporal metrics was implemented at the annual scale, which may overestimate errors due to the existence of urban renewal activities at the beginning (e.g. January) or end (e.g. December) of a year (Li et al. 2018). Thus, we conducted a second validation approach by allowing \pm one year deviation relative to the reference data. As Figure 6(d–f) illustrates, adopting the fuzzy true detection gives rise to substantial OA improvements, especially for ET (from 58.76% to 80.67%) and DUR (from 47.42% to 71.39%). Meanwhile, the other two error indicators (RMSE and SE) remain essentially stable, suggesting the one-year tolerance assessment is reasonable and necessary for this study.

3.2. Spatiotemporal patterns of urban renewal

3.2.1. Spatial distribution of urban renewal

Figure 7 shows the spatially continuous map of urban renewal distribution at a 30 m resolution from 1999 to 2019. Based on this map and probability sample data, we estimated that the total area of urban renewal within the study area is 340 ± 55 km² (95%

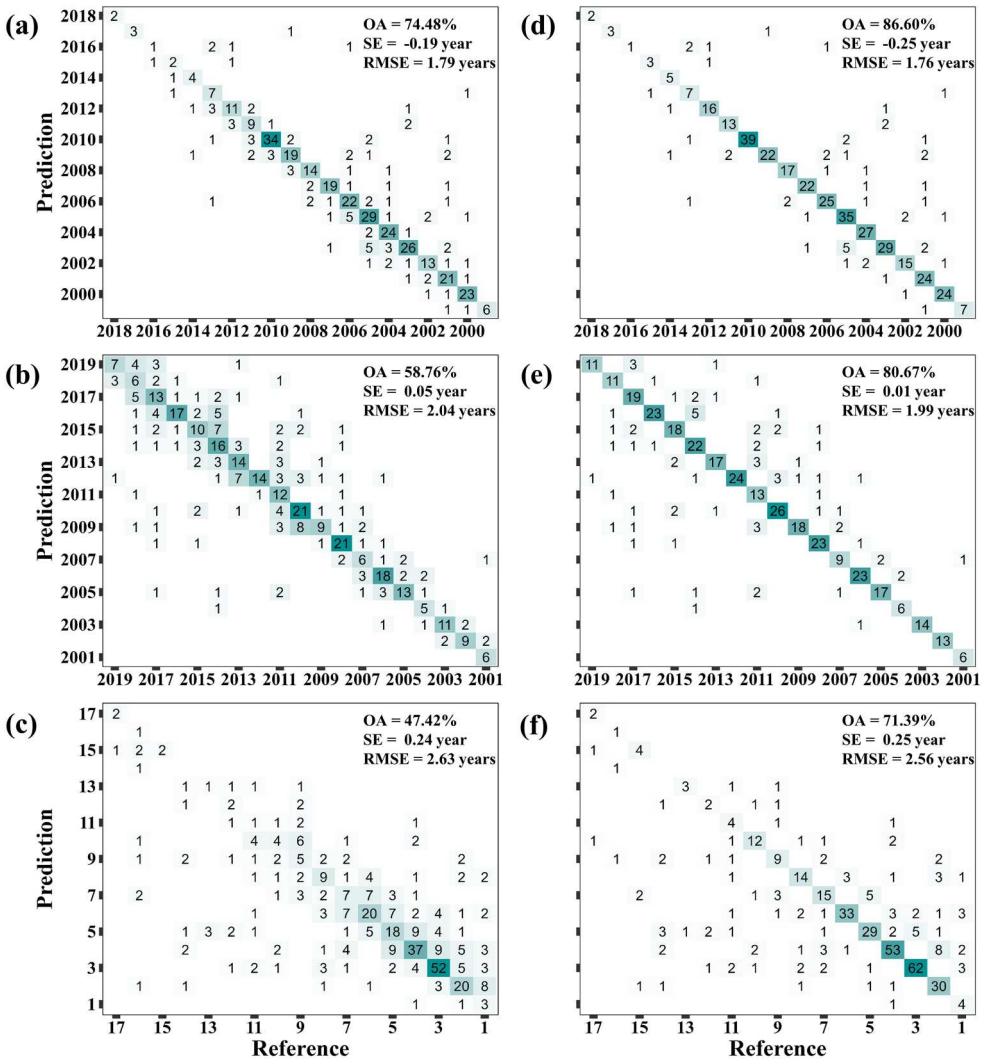


Figure 6. Performance evaluation of urban renewal temporal metrics. (a) ST performance using the exact-year strategy; (b) ET performance using the exact-year strategy; (c) DUR performance using the exact-year strategy; (d) ST performance using the one-year tolerance strategy; (e) ET performance using the one-year tolerance strategy; (f) DUR performance using the one-year tolerance strategy.

confidence interval), representing a 5.95% share of the entire Beijing urban space. Among other three pixel types, natural cover has the largest area ($2996 \pm 108 \text{ km}^2$), followed by stable urban ($1219 \pm 88 \text{ km}^2$) and urban expansion ($1146 \pm 98 \text{ km}^2$). Spatially, urban renewal clusters typically co-exist with persistent urban regions, forming a discontinuously circular distribution between the Second and Fifth Ring Roads of Beijing city (Figure 7(a)). This spatial pattern is consistent with a recent LandTrendr-based building change monitoring study (Hu et al. 2024), and reflects the gradual renovation of Beijing urban core areas during the past two decades driven by policies (Tu et al. 2023). For example, the entire neighborhood of Wukesong (located in HD) experienced

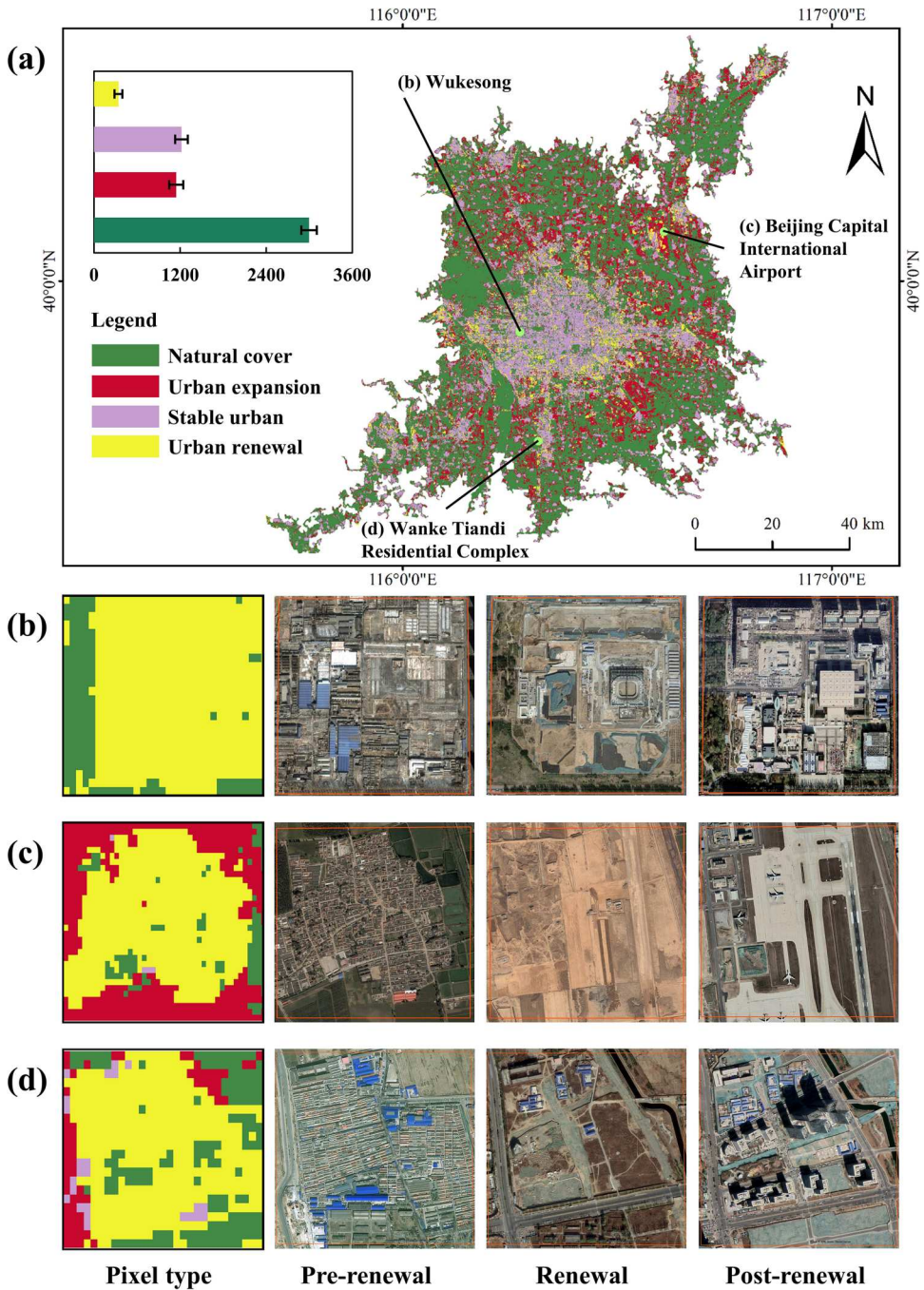


Figure 7. The map of urban renewal distribution for the study area. (a) Overall pattern of four pixel types (natural cover, urban expansion, stable urban and urban renewal) during 1999~2019. The insert bar chart shows the error-adjusted area estimate (km²) as well as the 95% confidence interval for each pixel type. (b), (c) and (d) are enlarged examples representing three urban renewal cases. The high resolution images are derived from Google Earth.

reconstruction from a residence community to a sports/leisure complex, and its distribution pattern was accurately captured by our map (Figure 7(b)). Our mapping result also suggests the presence of detectable renewal activities at urban fringes, which can be attributed to two primary reasons. First, the development of large-scale infrastructure requires considerable land resources from the surrounding built-up areas. Taking Beijing Capital International Airport as an instance, the extension project not only occupies croplands, but also existing artificial impervious surfaces. As a result, several settlements were demolished for the construction of the new terminal building and its ancillary facilities (Figure 7(c)). Second, real estate development may act as the other factor triggering the renewal of peri-urban regions. As illustrated in Figure 7(d), tearing down old residential areas provided considerable space for building a new residential community (Vanke Tiandi Residential Complex). Overall, our framework performs well in mapping urban renewal distribution within the study area.

We calculated area and percentage statistics of urban renewal distribution for 11 Beijing districts that are located within the study domain (Figure 8). As for the total urban renewal area, we found statistical results ranges from 3.76 km² (DC) to 58.12 km² (SY), suggesting a substantial spatial variation across different districts (Figure 8(a)). Interestingly, districts with large (greater than 25.70 km²) and small

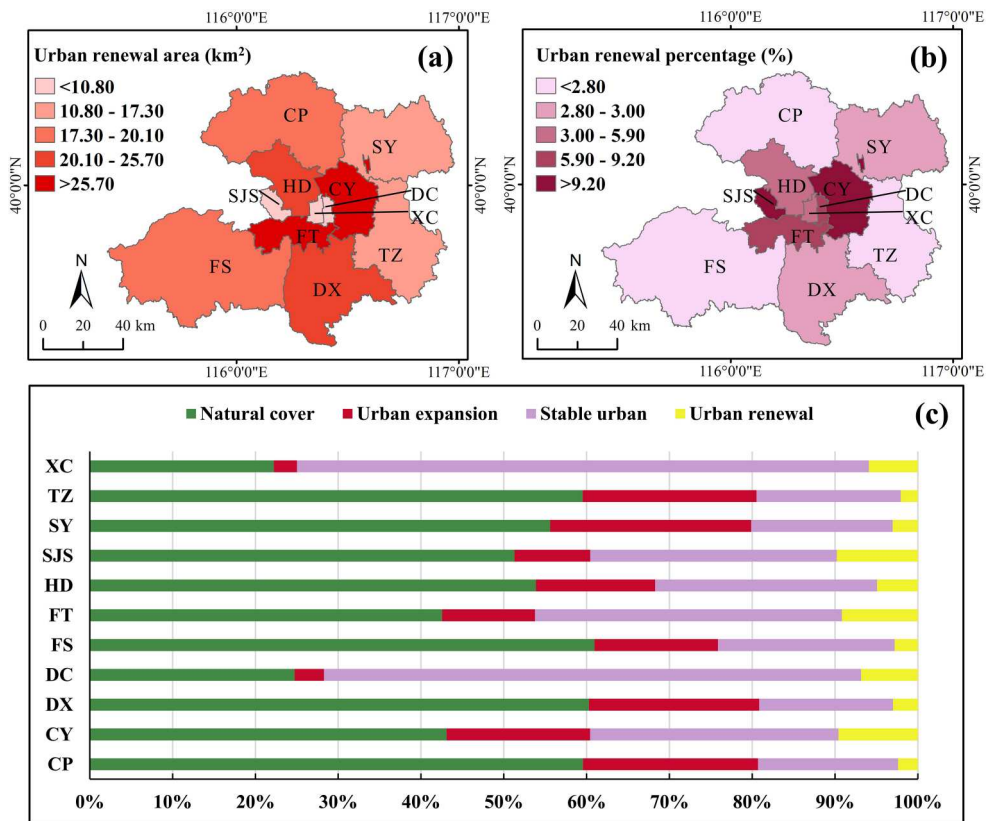


Figure 8. District based statistics of total urban renewal area (a), urban renewal percentage (b), and pixel type composition (c). District abbreviations are given in Section 2.1 of the main text.

urban renewal areas (less than 10.80 km^2) were concurrently observed in urban core regions. On the contrary, peri-urban districts exhibited medium-scale urban renewal area levels ($10.80\text{--}25.70 \text{ km}^2$). As for the urban renewal percentage, the distinction between urban core and peri-urban districts becomes even more evident (Figure 8(b)). Specifically, the highest urban renewal percentage was found in SJS (9.77%), tightly followed by SY and FT with over 9% of total area identified as urban renewal lands. In contrast, overall lower urban renewal percentage estimations were observed in three suburban districts with values of 2.06% (TZ), 2.38% (CP) and 2.79% (FS), respectively. Figure 8(c) further displays the composition of four pixel types for each district over the study years. In general, natural cover is the primary land use class, accounting for more than 40% of the total area in nine out of eleven districts (CP, CY, DX, FS, FT, HD, SJS, SY and TZ). Stable urban, on the other hand, prevails in the remaining two urban core districts (i.e. DC and XC). Of particular note is that in three districts (DC, SJS, and XC), the proportion of urban renewal areas is higher than that of urban expansion, highlighting the urbanization shift from spreading out to the renovation of existing built-up areas.

3.2.2. ST, ET and DUR of urban renewal

Figure 9 shows spatial and temporal distributions of estimated urban renewal time information within the study area. Blue tones in the predicted pixels are assigned to early ST/ET or short DUR while yellow and red tones indicate later ST/ET emergence or longer DUR. Non-renewal pixels are labeled as black color. For ST, we found a spatially explicit pattern extending from the city center to the outskirts (Figure 9(a)), with an average urban renewal beginning time of 2006.87 ± 4.76 years (one standard deviation, hereafter). More specifically, the earliest wave of urban renewal boom starting before 2005 was primarily observed within the Fifth Ring Road of Beijing city. This spatial distribution largely mirrors that of pixel clusters with later ST, most obviously identified in the peri-urban regions such as DX, SY and TZ. Temporally, the vast majority (78.34%) of urban renewal ST estimations were concentrated in the first decade of the twenty-first century, resulting in a decrease trend of ST occurrence over 1999–2019 ($-0.35\%/year$) (Figure 9(b)). As for ET, a later time estimation was observed for the entire study area (2012.11 ± 5.22 years). Spatially, the difference between urban core and peri-urban regions generally widens and becomes more discernible (Figure 9(c)), despite the existence of several patches which exhibited relatively early ET time but were characterized by suburban landscapes (e.g. Beijing Capital International Airport and its ancillary buildings). At the temporal domain, the second decade (2010~2019) exhibited a noteworthy ET occurrence acceleration than the first decade (1999~2009), leading to an observed increase of $0.34\%/year$ (Figure 9(d)). The spatiotemporal patterns of DUR reflect the joint impacts of ST and ET (Figure 9(e, f)). Overall, the mean and standard derivation of the durations of all detected urban renewal activities were 5.33 and 4.59 years, respectively, indicating the dominance of ‘quick demolition and quick reconstruction’ across the study area. By binning the DUR map into a histogram, we found that nearly half (48.16%) of the renewal pixels have DUR estimations equal or less than five years, giving rise to a downward trend of the frequency distribution. Figure 8(g) further displays the zoom-in views of estimated urban renewal temporal metric maps by selecting three regional subsets, each of which represents one typical landscape environment. For Beijing

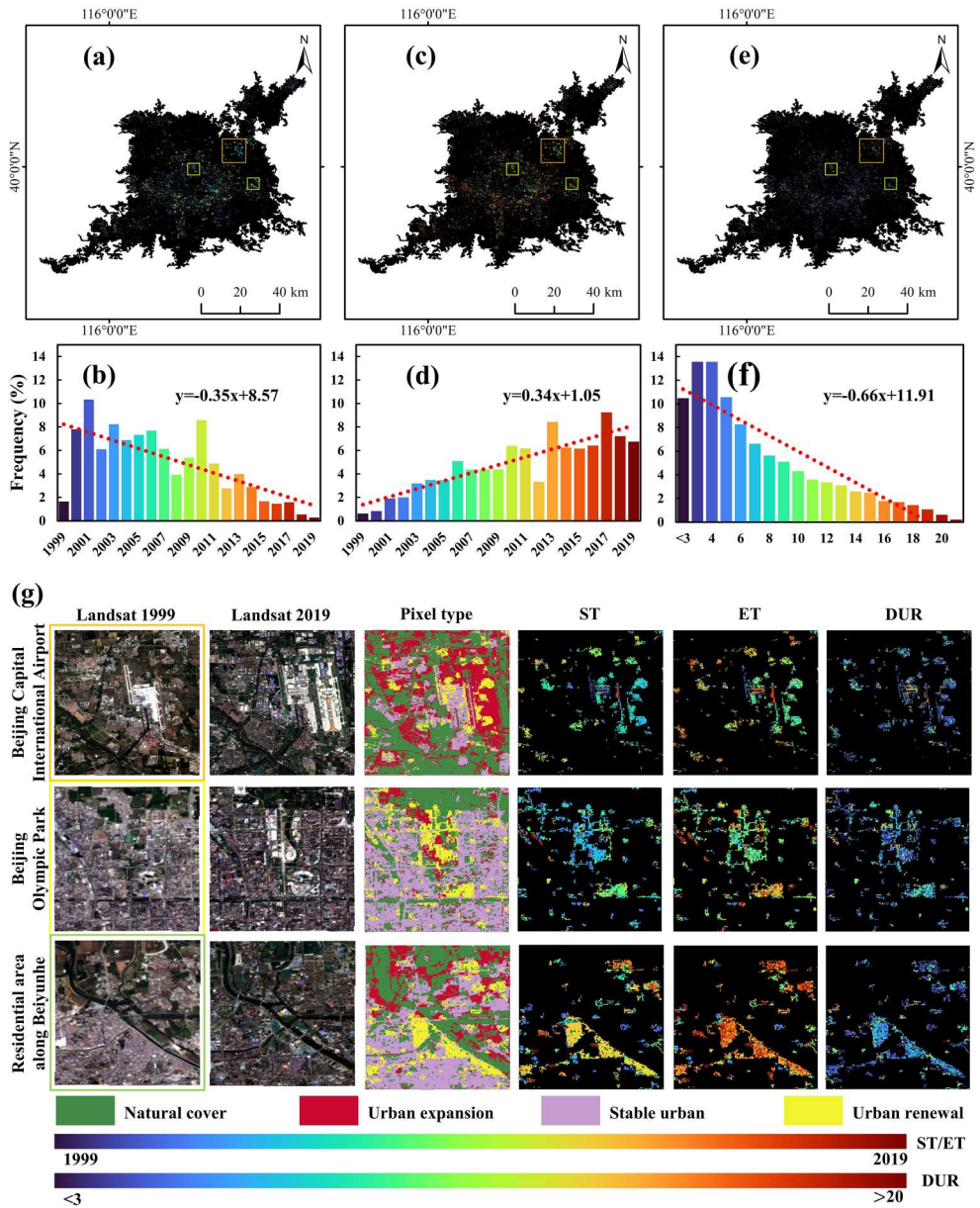


Figure 9. Spatial and temporal distributions of estimated urban renewal time information within the study area. (a), (b), (c) are spatially continuous maps of ST, ET and DUR. (d), (e), (f) are histograms of ST, ET and DUR maps, respectively. The red dotted line shows the simple linear regression line. (g) shows zoomed-in views of urban renewal information extraction results for three regional subsets. True color Landsat images acquired in 1999 and 2019 are used for visual interpretation. Noted that all results are displayed at the annual scale.

Capital International Airport, we found most renewal activities began as early as 2004 and ended before 2008, resulting in durations less than five years. These estimations echo the timeline of the airport terminal area expansion project. Comparatively, living

buildings outside of the airport exhibited later ST and ET but similar DUR outcomes. Beijing Olympic Park is a typical example of urban renewal promoted by national events. Our results show that the demolition of old settlements and the following reconstruction mainly occurred over 2002–2007, in accordance with the preparation for the 2008 Summer Olympics and the 2008 Summer Paralympics. In addition to sports venues, we also noticed patches rebuilt for other purposes, most of which exhibited later ET and longer DUR estimations. Our maps also provide spatiotemporal insights into the effect of real estate development on urban renewal. For instance, the old residential areas along the Beiyunhe river experienced a large-scale demolition process around 2010, followed by construction of new residential quarters until the end years of the study period.

There also exist differences in three urban renewal temporal metrics across the eleven districts (Figure 10), which are subject to varying geographical and socio-economic factors such as topography, policy and financial conditions. In general, our results show a greater intra-district variation of ET (typically range from 2005 to 2016) than that of ST (typically range from 2003 to 2010). Diving deeper into the box-plots, we find overall earlier ST in DC, XC, and HD with mean values of 2005.43, 2005.49, and 2006.24, respectively. Moreover, DC and XC also exhibit earlier ET results with mean values of 2009.22 and 2009.84. Conversely, other districts have relatively late urban renewal beginning and ending time. In comparison with ST and ET, the statistical distribution of DUR has the highest level of intra-district agreement and concentration. Specifically, the mean DUR values vary from 3.79 to 5.80 years across districts, despite the presence of a few outliers that exhibit longer urban renewal durations.

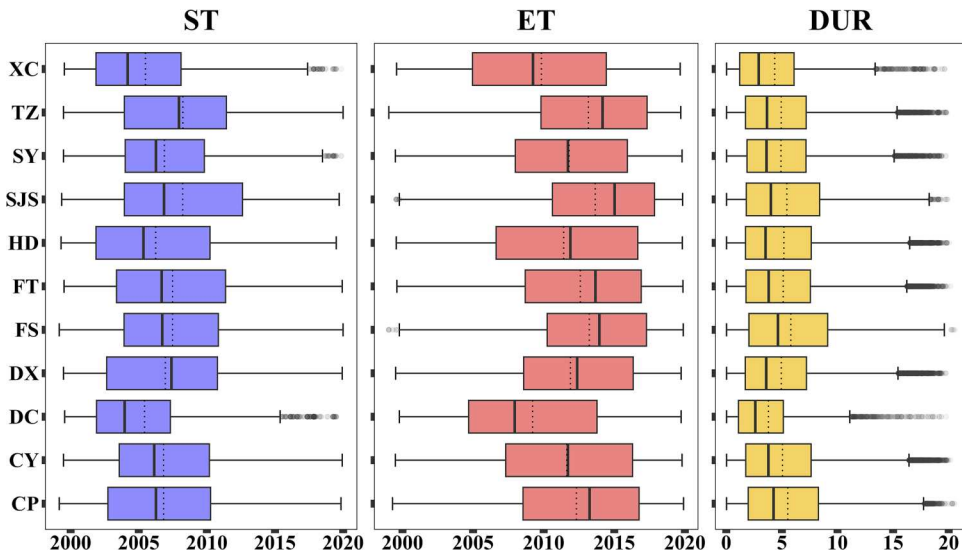


Figure 10. District based statistics of urban renewal temporal metrics including ST, ET, and DUR. The whiskers and boxes indicate the minimum, 25th percentile, median, 75th percentile, and maximum, while the dotted lines represent the mean values. Outliers are displayed as points. The district abbreviations are given in Section 2.1 of the main text.

4. Discussion

4.1. Advantages of the proposed algorithm framework

The ongoing worldwide urbanization brings accelerated demands for housing, infrastructure, and public services. Urban renewal plays a more important role than ever in meeting these demands, particularly in densely populated areas with constrained land availability (Nachmany and Hananel 2023). Therefore, accurate mapping of urban renewal spatiotemporal patterns is essential for understanding the ‘human-land-city’ nexus and achieving sustainable development. Notwithstanding recent progress in urbanization monitoring from space, urban renewal identification relying on remote sensing techniques still stands out as a challenging task (Ni et al. 2023; Zhao et al. 2023; Hu et al. 2024). Although supervised classification is a widely used strategy for land surface mapping, isolating urban renewal from other LCLUC types requires reference data in terms of both land cover labels and land cover change categories, making it difficult to collect sufficient reliable sample for model training and calibration (Ni, Yu, and Gong 2024). Moreover, the renewal process of existing built-up areas involves complex and varied land covers such as bare soil (Zhao, Xia, and Li 2023), vegetation (Zhuo et al. 2024), and reconstruction site with/without dust-proof net (Zhang, Chen, et al. 2024), all of which are associated with high spectral and spatial heterogeneity. To address these challenges, we developed a framework that leveraged dense Landsat time-series information from the pre-computed global CCD segments dataset for urban renewal mapping and temporal metrics estimation. Based on the sample migration theory, this framework created a consistent training dataset for classifying the land cover type of each CCD time segment during the study period, which allowed us to identify the per-pixel existence of urban renewal. The recorded disturbances (i.e. breakpoints between two adjacent time segments), on the other hand, were utilized for estimating three temporal metrics of urban renewal including ST, ET and DUR. We evaluated the generated urban renewal maps and found overall satisfactory performances at the spatial and temporal domains (Table 1, Figure 6).

Our framework offers three key advantages. First, unlike traditional urbanization monitoring methods that rely heavily on satellite image collection or manual input selection, our approach requires only Landsat-based CCD segments and minimal auxiliary datasets (Figure 3). This enhances generalizability in urban renewal mapping while reducing data dependency. By leveraging stable pixels identified by CCD, training data can be directly derived from existing land cover maps (e.g. WorldCover 2020) for RFC development. Additionally, classified CCD segments enable the integration of prior knowledge rules to improve urban renewal detection. Second, our framework provides per-pixel estimates of urban renewal timing (including ST, ET, and DUR) enabling precise tracking of land-use changes. These metrics not only facilitate reconstruction history analysis but also offer insights into the socio-economic and environmental impacts of urban renewal. For instance, rapid renewal processes differ significantly from gradual ones, with distinct implications for urban development (Nachmany and Hananel 2023; Zhao et al. 2023). Third, despite being tested in a single city, the framework is designed for scalability. The CCD segment classification can be adapted using locally optimized strategies (Liu, Huang, et al. 2024), while renewal mapping and temporal metric extraction require only minor parameter adjustments (e.g. *Ind*). By implementing the framework on the

GEE platform, we further demonstrate its feasibility for large-area applications, capitalizing on cloud computing advancements.

Several studies have explored LCLUC mapping techniques relevant to urban renewal. For instance, Zhuo et al. (2024) employed annual Landsat time series to distinguish renewed and non-renewed buildings, subsequently applying their method to estimate building ages. Similarly, Ni, Yu, and Gong (2024) recently adopted a comparable approach to map old and renewed urban areas across China. Beyond time-series-based methods, alternative strategies, such as thresholding (Qiao et al. 2020), supervised classification (Zhao, Chen, et al. 2023; Zhao, Xia, and Li 2023), and spectral mixture analysis (Yue et al. 2006) have been utilized to detect built-up area demolition and reconstruction. Building upon these advancements, our study introduces a new paradigm for deriving urban renewal distribution, timing, and duration. Unlike prior works that focus solely on building renewal (Wang et al. 2023), our framework applies to multiple built-up classes, enabling more comprehensive urban renewal assessment. Furthermore, we advance beyond traditional binary (renewal/non-renewal) classification by categorizing urban land development into four distinct types: natural cover, urban expansion, stable urban and urban renewal. This refined classification captures subtle landscape heterogeneity more effectively. Additionally, the continuous monitoring capability of CCD allows for temporal urban renewal analysis at flexible time scales, a significant improvement over static approaches. In summary, our framework complements and enhances existing methods, providing a timely, cost-effective, and spatially detailed approach to understanding urban renewal dynamics.

4.2. Uncertainties influencing the accuracy of urban renewal information extraction

While the developed framework has attractive qualities with respect to urban renewal information extraction, our study also indicates several issues that warrant further attention. After applying the one-year tolerance strategy, the generated urban renewal maps exhibited spatial and temporal accuracies with achieved OAs over 70% (Table 1, Figure 6). The remaining errors may stem from uncertainties in the input data and limitations within the algorithm framework. For this work, we utilized the CCD segments product as the primary data source, which provides band-specific surface reflectance modeling parameters and identifies statistical breaks based on two decades' worth of Landsat satellite archives. Despite the well-recognized capacity for land surface monitoring, CCD was reported to be less informative for detecting small change magnitude or extremely rapid disturbances (Cohen et al. 2017; Zhu et al. 2020). Additionally, the parameterization of CCD can influence its performance, as variations in threshold settings (e.g. chi-square probability) and model fitting constraints (e.g. minimum observations) directly affect sensitivity to land surface changes and false alarm rates (Pasquarella et al. 2022). This issue becomes more critical in urban areas characterized by heterogeneous land cover distribution and configuration, giving rise to the presence of mixed spectral signatures that can lead to a decreased change detection accuracy (Liu et al. 2019). On the other hand, not all detected changes by CCD correspond to actual disturbances, but rather spectral deviation events due to climatic variability or repeated cloud coverage (Bullock, Woodcock, and Holden 2020; Xian et al. 2022). As a consequence, we can

expect a reduced user's accuracy of the predicted urban renewal existence map (Table 1), even after a refinement procedure included in the decision tree model. Another major concern originates from the reference land cover map. Based on a global validation dataset, Xu et al. (2024) showed that WorldCover 2020 has a relatively undesirable mapping performance in built-up areas compared with other natural environments. The misclassification errors may be propagated into the constructed training sample set, which will probably influence the mapping results. Additionally, there is a temporal mismatch (i.e. a two-year gap) between the used urban boundary dataset (GUB 2018) and WorldCover 2020, adding extra uncertainty into our algorithm framework. Given the capacity of tracking urban changes at a high spatial resolution, Google Earth historical images offer the most valuable information for urban renewal mapping validation. However, these pre-acquired images are not evenly distributed over space and through time, making the reference data less representative across the entire study area.

Methodologically, each component of the current framework is associated with factors that can affect the accuracy of urban renewal information extraction. It is important to note that urban renewal can manifest in diverse forms. However, since this study specifically confines the scope of urban renewal to the comprehensive process of built-up land demolition and reconstruction, the proposed framework is anticipated to have limited applicability in monitoring non-land-replacing urban renewal activities, such as functional upgrades and building renovations. Moreover, within several cities in China, it is common practice to tear down old blocks and plant vegetations for green space (Li et al. 2023). Such an urban greening process was simply identified as the natural cover, causing our results less informative in these special areas. As a key step in generating per-pixel land cover time series profile, segments classification in this study was implemented by RFC. Although this machine learning algorithm has been widely adopted in the field of land cover mapping, it depends heavily on the sampling design (Belgiu and Drăguț 2016) and input feature selection (Liu, Wu, et al. 2025), resulting in inconsistent classification performances under various geographical conditions. During the procedure of urban renewal existence mapping, the most challenging part lies in the treatment of pixels with only one CCD-detected change. Due to the lack of land cover profile information, stable built-up lands can be easily confused with those experiencing renewal activities. We attempted to reduce this confusion by adopting a threshold-based method, which was shown to be useful within the study area. Nevertheless, the determination of the threshold may require further improvement using more available sample points, especially when applied to a large spatial extent. In this study, we selected the widely-used Landsat band, SWIR1, for capturing the temporal characteristics of urban renewal, which could be different from those identified by alternative spectral bands or indices. Hu et al. (2024) discovered that different spectral indicators varied in their effectiveness at accurately detecting building disturbance signals, with SWIR1 and SWIR2 performing more effectively than the normalized difference built-up index (NDBI) (Y. Zha, Gao and Ni 2003) or modified normalized difference water index (MNDWI) (Xu 2006). Finally, although the developed framework predicts the time points of demolition and reconstruction in a continuous way, their accuracy evaluations were performed at the annual scale. Such a temporal scale mismatch may also lead to additional uncertainties embedded in error indicators.

4.3. Driving forces, political implications, and future work

The spatiotemporal patterns of urban renewal in Beijing city reflect the interplay of policy, economic, and socio-environmental factors, with significant implications for sustainable urban development. As shown in our mapping results (Figure 7~9), renewal hotspots inside the Fifth Ring Road were shaped strongly by government policies and economic incentives typified by the 2008 Olympics-driven redevelopment (Ren 2011) in CY and DC, which led to earlier ST and faster completions. Conversely, districts like SY in the outer fringes proceeded more slowly, possibly due to weaker policy focus or lower real-estate demand. Overall, government-led initiatives (e.g. old city redevelopment) and market forces fostered a ‘quick demolition – reconstruction’ pattern (mean DUR = 5.33 years). Yet, outliers also revealed inequities, particularly in peri-urban areas, where the process often took over 10 years (see Figure 10). The delayed reconstruction can be attributed to a number of reasons, such as land use history, funding shortage, and policy regulations. Unfinished reconstruction sites will give rise to a series of environmental issues including air pollution, noise, and soil degradation, which contribute to urbanization challenges and in turn, affect land use planning and development decisions. Our study provides observational evidence of such information and therefore helps to encourage city infrastructure equity, a task that is critical and urgent for sustainable urban development (Zhao et al. 2024). Based on microwave backscatter data, several pioneering studies reported a notable shift of global urban development from horizontal expansion to vertical growth, and linked this trend to various driving factors (Mahtta, Mahendra, and Seto 2019; Froelking et al. 2022, 2024). In this study, we detected the removal of low-rise buildings followed by constructing high-rise ones (Figures 7 and 9), which is consistent with the transition. The change of urban form in its vertical direction not only affects population density (Li, Zhou, et al. 2020; Wang et al. 2023), but also influences microclimate, energy consumption, and greenhouse gas emissions (Creutzig et al. 2015; Ratti, Baker, and Steemers 2005; Zhou et al. 2022).

Using this study as the baseline, future endeavors can be emphasized in terms of the following aspects. First and foremost, newly emerging geospatial data and algorithms should be integrated with the presented framework to enhance the performance of urban renewal information extraction. In this study, we implemented our framework primarily based on three global datasets (Landsat-based CCD segments, GUB 2018 and WorldCover 2020). However, their reliabilities are not evenly distributed over space, making them less representative for the targeted study area. Therefore, it is essential to optimize the data source selection by utilizing a diverse range of complementary products at local scales, while ensuring that the integration is carefully designed and systematically implemented (Liu, Zhang, et al. 2020). Moreover, the training sample set can be improved by migrating prior knowledge from multiple sources including high-quality land cover products (Liu, Wu, et al. 2025), global sample libraries (Huang et al. 2020), street view imagery (Zhang et al. 2019) and social media such as point-of-interest (POI) records (Chen et al. 2021). Considering generalizability, computational costs, and interpretability, the proposed algorithm framework was implemented using classic machine learning models (RFC and decision tree). With the rapid development of artificial intelligence and computing technologies, we anticipate that deep learning-based

methods in the near future will further improve urban renewal monitoring performance aided by massive sample resources (Li et al. 2024). Second, rather than per-pixel information extraction, further studies should focus on the implementation of urban renewal monitoring at the street block level, a mapping unit representing relatively homogeneous urban functions as well as their dynamics (Chen et al. 2021; Xiong et al. 2024). This modification is expected to not only improve the mapping/estimating reliability by incorporating spatially context properties such as texture (Ye, Zhu, and Cao 2023), but also facilitate in-depth analyses of urban renewal including its type, agent, and possible impacts. Third, there is a pressing need to extend the urban renewal monitoring efforts from a single city to broader scales. Due to inherent differences in geographical and socio-economic conditions, we may expect substantial spatio-temporal pattern discrepancies of urban renewal across regions and countries. Such knowledge is not fully reflected in existing remote sensing datasets, yet crucial for us to prioritize efforts on achieving the sustainable development goals both locally and globally. Finally, Future work could merge socio-economic data (e.g. real-estate prices, GDP growth) with these remote-sensing findings, enabling planners to better decode the forces driving uneven renewal speeds and design more balanced revitalization strategies that align temporal metrics (ST/ET/DUR) with socio-economic equity goals.

5. Conclusions

Urban renewal represents an emerging opportunity to ensure cities meeting the requirements of modern populations by revitalizing deteriorate infrastructures. Although there have been remote sensing studies focusing on urban LCLUC, accurate urban renewal characterization from space still remains an unsolved challenge, which hampers our capacity to project the long-term sustainability of urban environments. Therefore, in this study, we proposed an algorithm framework for deriving the distribution, timing, and duration of urban renewal by leveraging dense time-series information derived from the Landsat-based CCD segments dataset. The proposed framework is applicable to various built-up classes, enabling a more comprehensive assessment of urban renewal. Unlike traditional binary (renewal vs. non-renewal) approaches, our method categorizes urban land development into four distinct types, effectively capturing nuanced patterns in heterogeneous landscapes. Furthermore, the continuous monitoring capability of CCD facilitates the estimation of urban renewal temporal metrics at any desired temporal resolution.

The proposed framework was implemented and evaluated in Beijing city where considerable efforts have been made on the reconstruction of existing built-up areas during the study years. Accuracy assessments confirmed the feasibility of the framework, with OAs of 82.36% and 71.39~86.60% (one-year tolerance strategy) at the spatial and temporal domains, respectively. Following this framework, we estimated that the total urban renewal area of the study domain reaches 340 ± 55 km² during the period 1999~2019, which is unevenly distributed among districts in Beijing. Despite the urban-rural gradient in ST and ET trends, we found a relatively homogeneous DUR pattern, with nearly half of detected urban renewal activities accomplished within five years. While the framework currently focuses on land-replacing renewal and confronts uncertainties in input datasets, these limitations can be overcome by integrating

multi-sensor data and deep learning models. Such advancements would not only expand detection to non-physical renewal but also improve robustness across diverse city types, thus enabling globally scalable monitoring for evidence-based urban governance.

Acknowledgements

The authors would like to thank the editors and anonymous reviewers for their constructive and insightful comments on an earlier draft of this paper.

Disclosure statement

No potential conflict of interest was reported by the author(s).

Funding

This study was supported by the National Natural Science Foundation of China (42371344).

Data availability statement

All data supporting this study are available from the corresponding author upon reasonable request.

ORCID

Qi Zhang  <http://orcid.org/0000-0002-4242-7614>

References

- Acuto, Michele, Susan Parnell, and Karen C. Seto. 2018. "Building a Global Urban Science." *Nature Sustainability* 1 (1): 2–4. <https://doi.org/10.1038/s41893-017-0013-9>.
- Ahmadian, Ehsan, Behzad Sodagar, Chris Bingham, Amira Elnokaly, and Glen Mills. 2021. "Effect of Urban Built Form and Density on Building Energy Performance in Temperate Climates." *Energy and Buildings* 236:110762. <https://doi.org/10.1016/j.enbuild.2021.110762>.
- Arévalo, Paulo, Eric L. Bullock, Curtis E. Woodcock, and Pontus Olofsson. 2020. "A Suite of Tools for Continuous Land Change Monitoring in Google Earth Engine." *Frontiers in Climate* 2 (26): 576740. <https://doi.org/10.3389/fclim.2020.576740>.
- Bansal, Parth, and Steven Jige Quan. 2022. "Relationships between Building Characteristics, Urban Form and Building Energy use in Different Local Climate Zone Contexts: An Empirical Study in Seoul." *Energy and Buildings* 272:112335. <https://doi.org/10.1016/j.enbuild.2022.112335>.
- Belgiu, Mariana, and Lucian Drăguț. 2016. "Random Forest in Remote Sensing: A Review of Applications and Future Directions." *ISPRS Journal of Photogrammetry and Remote Sensing* 114:24–31. <https://doi.org/10.1016/j.isprsjprs.2016.01.011>.
- BMBS. 2020. *Beijing Statistical Yearbook 2020*. Beijing Municipal Bureau of Statistics. <https://nj.tjj.beijing.gov.cn/nj/main/2020-tjn/zk/e/indexee.htm>.
- Breiman, Leo. 2001. "Random Forests." *Machine Learning* 45 (1): 5–32. <https://doi.org/10.1023/A:1010933404324>.
- Bullock, Eric L., Curtis E. Woodcock, and Christopher E. Holden. 2020. "Improved Change Monitoring Using an Ensemble of Time Series Algorithms." *Remote Sensing of Environment* 238:111165. <https://doi.org/10.1016/j.rse.2019.04.018>.

- Che, Yangzi, Xuecao Li, Xiaoping Liu, Xiaocong Xu, Kangning Huang, Peng Zhu, Qian Shi, et al. 2024. "Mapping of Individual Building Heights Reveals the Large gap of Urban-Rural Living Spaces in the Contiguous US." *The Innovation Geoscience* 2 (2): 100069. <https://doi.org/10.59717/j.xinn-geo.2024.100069>.
- Chen, Bin, Ying Tu, Yimeng Song, David M. Theobald, Tao Zhang, Zhehao Ren, Xuecao Li, et al. 2021. "Mapping Essential Urban Land use Categories with Open big Data: Results for Five Metropolitan Areas in the United States of America." *ISPRS Journal of Photogrammetry and Remote Sensing* 178:203–218. <https://doi.org/10.1016/j.isprsjprs.2021.06.010>.
- Cohen, Warren B., Sean P. Healey, Zhiqiang Yang, Stephen V. Stehman, C. Kenneth Brewer, Evan B. Brooks, Noel Gorelick, et al. 2017. "How Similar Are Forest Disturbance Maps Derived from Different Landsat Time Series Algorithms?" *Forests* 8 (4): 98. <https://doi.org/10.3390/f8040098>.
- Cohen, Warren B., Zhiqiang Yang, Sean P. Healey, Robert E. Kennedy, and Noel Gorelick. 2018. "A LandTrendr Multispectral Ensemble for Forest Disturbance Detection." *Remote Sensing of Environment* 205:131–140. <https://doi.org/10.1016/j.rse.2017.11.015>.
- Creutzig, Felix, Giovanni Baiocchi, Robert Bierkandt, Peter-Paul Pichler, and Karen C. Seto. 2015. "Global Typology of Urban Energy use and Potentials for an Urbanization Mitigation Wedge." *Proceedings of the National Academy of Sciences* 112 (20): 6283–6288. <https://doi.org/10.1073/pnas.1315545112>.
- Dannenberg, Matthew P., Christopher R. Hakkenberg, and Conghe Song. 2016. "Consistent Classification of Landsat Time Series with an Improved Automatic Adaptive Signature Generalization Algorithm." *Remote Sensing* 8 (8): 691. <https://doi.org/10.3390/rs8080691>.
- Frolking, Steve, Richa Mahtta, Tom Milliman, Thomas Esch, and Karen C. Seto. 2024. "Global Urban Structural Growth Shows a Profound Shift from Spreading Out to Building up." *Nature Cities* 1 (9): 555–566. <https://doi.org/10.1038/s44284-024-00100-1>.
- Frolking, Steve, Tom Milliman, Richa Mahtta, Aaron Paget, David G. Long, and Karen C. Seto. 2022. "A Global Urban Microwave Backscatter Time Series Data set for 1993–2020 Using ERS, QuikSCAT, and ASCAT Data." *Scientific Data* 9 (1): 88. <https://doi.org/10.1038/s41597-022-01193-w>.
- Gong, Peng, Xuecao Li, Jie Wang, Yuqi Bai, Bin Chen, Tengyun Hu, Xiaoping Liu, et al. 2020. "Annual Maps of Global Artificial Impervious Area (GAIA) between 1985 and 2018." *Remote Sensing of Environment* 236:111510. <https://doi.org/10.1016/j.rse.2019.111510>.
- Gong, Peng, Song Liang, Elizabeth J. Carlton, Qingwu Jiang, Jianyong Wu, Lei Wang, and Justin V. Remais. 2012. "Urbanisation and Health in China." *The Lancet* 379 (9818): 843–852. [https://doi.org/10.1016/S0140-6736\(11\)61878-3](https://doi.org/10.1016/S0140-6736(11)61878-3).
- Gorelick, Noel, Matt Hancher, Mike Dixon, Simon Ilyushchenko, David Thau, and Rebecca Moore. 2017. "Google Earth Engine: Planetary-Scale Geospatial Analysis for Everyone." *Remote Sensing of Environment* 202:18–27. <https://doi.org/10.1016/j.rse.2017.06.031>.
- Gorelick, Noel, Zhiqiang Yang, Paulo Arévalo, Eric L. Bullock, Katherin Patricia Insfrán, and Sean P. Healey. 2023. "A Global Time Series Dataset to Facilitate Forest Greenhouse Gas Reporting." *Environmental Research Letters* 18 (8): 084001. <https://doi.org/10.1088/1748-9326/ace2da>.
- Gray, Josh, and Conghe Song. 2013. "Consistent Classification of Image Time Series with Automatic Adaptive Signature Generalization." *Remote Sensing of Environment* 134:333–341. <https://doi.org/10.1016/j.rse.2013.03.022>.
- Grimm, Nancy B., Stanley H. Faeth, Nancy E. Golubiewski, Charles L. Redman, Jianguo Wu, Xuemei Bai, and John M. Briggs. 2008. "Global Change and the Ecology of Cities." *Science* 319 (5864): 756–760. <https://doi.org/10.1126/science.1150195>.
- Hashemi-Parast, S. Omid, Fumio Yamazaki, and Wen Liu. 2017. "Monitoring and Evaluation of the Urban Reconstruction Process in Bam, Iran, after the 2003 Mw 6.6 Earthquake." *Natural Hazards* 85 (1): 197–213. <https://doi.org/10.1007/s11069-016-2573-9>.
- He, Tingting, Yihua Hu, Andong Guo, Yuwei Chen, Jun Yang, Mengmeng Li, and Maoxin Zhang. 2024. "Quantifying the Impact of Urban Trees on Land Surface Temperature in Global Cities." *ISPRS Journal of Photogrammetry and Remote Sensing* 210:69–79. <https://doi.org/10.1016/j.isprsjprs.2024.03.007>.

- Hermosilla, Txomin, Michael A. Wulder, Joanne C. White, Nicholas C. Coops, Geordie W. Hobart, and Lorraine B. Campbell. 2016. "Mass Data Processing of Time Series Landsat Imagery: Pixels to Data Products for Forest Monitoring." *International Journal of Digital Earth* 9 (11): 1035–1054. <https://doi.org/10.1080/17538947.2016.1187673>.
- Hu, Tengyun, Meng Zhang, Xuecao Li, Tinghai Wu, Qiwei Ma, Jianneng Xiao, Xieqin Huang, Jinchun Guo, Yangchun Li, and Donglie Liu. 2024. "Extraction of Building Construction Time Using the LandTrendr Model with Monthly Landsat Time Series Data." *IEEE Journal of Selected Topics in Applied Earth Observations and Remote Sensing* 17: 18335–18350. <https://doi.org/10.1109/JSTARS.2024.3409157>.
- Huang, Chengquan, Samuel N. Goward, Jeffrey G. Masek, Nancy Thomas, Zhiliang Zhu, and James E. Vogelmann. 2010. "An Automated Approach for Reconstructing Recent Forest Disturbance History Using Dense Landsat Time Series Stacks." *Remote Sensing of Environment* 114 (1): 183–198. <https://doi.org/10.1016/j.rse.2009.08.017>.
- Huang, Huabing, Jie Wang, Caixia Liu, Lu Liang, Congcong Li, and Peng Gong. 2020. "The Migration of Training Samples towards Dynamic Global Land Cover Mapping." *ISPRS Journal of Photogrammetry and Remote Sensing* 161:27–36. <https://doi.org/10.1016/j.isprsjprs.2020.01.010>.
- Kennedy, Robert E., Zhiqiang Yang, Justin Braaten, Catharine Copass, Natalya Antonova, Chris Jordan, and Peder Nelson. 2015. "Attribution of Disturbance Change Agent from Landsat Time-Series in Support of Habitat Monitoring in the Puget Sound Region, USA." *Remote Sensing of Environment* 166:271–285. <https://doi.org/10.1016/j.rse.2015.05.005>.
- Kennedy, Robert E., Zhiqiang Yang, and Warren B. Cohen. 2010. "Detecting Trends in Forest Disturbance and Recovery Using Yearly Landsat Time Series: 1. LandTrendr — Temporal Segmentation Algorithms." *Remote Sensing of Environment* 114 (12): 2897–2910. <https://doi.org/10.1016/j.rse.2010.07.008>.
- Li, Ziming, Bin Chen, Shengbiao Wu, Mo Su, Jing M. Chen, and Bing Xu. 2024. "Deep Learning for Urban Land use Category Classification: A Review and Experimental Assessment." *Remote Sensing of Environment* 311:114290. <https://doi.org/10.1016/j.rse.2024.114290>.
- Li, Xuecao, Peng Gong, Yuyu Zhou, Jie Wang, Yuqi Bai, Bin Chen, Tengyun Hu, et al. 2020. "Mapping Global Urban Boundaries from the Global Artificial Impervious Area (GAIA) Data." *Environmental Research Letters* 15 (9): 094044. <https://doi.org/10.1088/1748-9326/ab9be3>.
- Li, Long, Wenfeng Zhan, Weimin Ju, Josep Peñuelas, Zaichun Zhu, Shushi Peng, Xiaolin Zhu, et al. 2023. "Competition between Biogeochemical Drivers and Land-Cover Changes Determines Urban Greening or Browning." *Remote Sensing of Environment* 287:113481. <https://doi.org/10.1016/j.rse.2023.113481>.
- Li, Xuecao, Yuyu Zhou, Peng Gong, Karen C. Seto, and Nicholas Clinton. 2020. "Developing a Method to Estimate Building Height from Sentinel-1 Data." *Remote Sensing of Environment* 240:111705. <https://doi.org/10.1016/j.rse.2020.111705>.
- Li, Xuecao, Yuyu Zhou, Zhengyuan Zhu, Lu Liang, Bailang Yu, and Wenting Cao. 2018. "Mapping Annual Urban Dynamics (1985–2015) Using Time Series of Landsat Data." *Remote Sensing of Environment* 216:674–683. <https://doi.org/10.1016/j.rse.2018.07.030>.
- Liu, Han, Peng Gong, Jie Wang, Xi Wang, Grant Ning, and Bing Xu. 2021. "Production of Global Daily Seamless Data Cubes and Quantification of Global Land Cover Change from 1985 to 2020 - IMap World 1.0." *Remote Sensing of Environment* 258:112364. <https://doi.org/10.1016/j.rse.2021.112364>.
- Liu, Xiaoping, Yinghuai Huang, Xiaocong Xu, Xuecao Li, Xia Li, Philippe Ciais, Peirong Lin, et al. 2020. "High-spatiotemporal-resolution Mapping of Global Urban Change from 1985 to 2015." *Nature Sustainability* 3 (7): 564–570. <https://doi.org/10.1038/s41893-020-0521-x>.
- Liu, Chong, Huabing Huang, Qi Zhang, Xuejie Feng, Xuejiao Hou, Caixia Liu, Hanzeyu Xu, and Xiao Cheng. 2024. "Fine-resolution Mapping and Assessment of Artificial Surfaces in the Northern Hemisphere Permafrost Environments." *International Journal of Digital Earth* 17 (1): 2302579. <https://doi.org/10.1080/17538947.2024.2302579>.

- Liu, Guiwen, Lizhen Wei, Jianping Gu, Tao Zhou, and Yong Liu. 2020. "Benefit Distribution in Urban Renewal from the Perspectives of Efficiency and Fairness: A Game Theoretical Model and the Government's Role in China." *Cities* 96:102422. <https://doi.org/10.1016/j.cities.2019.102422>.
- Liu, Xiaoping, Xinxin Wu, Xuecao Li, Xiaocong Xu, Weilin Liao, Limin Jiao, Zhenzhong Zeng, Guangzhao Chen, and Xia Li. 2025. "Global Mapping of Three-Dimensional (3D) Urban Structures Reveals Escalating Utilization in the Vertical Dimension and Pronounced Building Space Inequality." *Engineering* 47: 86–99. <https://doi.org/10.1016/j.eng.2024.01.025>.
- Liu, Chong, Qi Zhang, Hui Luo, Shuhua Qi, Shiqi Tao, Hanzeyu Xu, and Yuan Yao. 2019. "An Efficient Approach to Capture Continuous Impervious Surface Dynamics Using Spatial-Temporal Rules and Dense Landsat Time Series Stacks." *Remote Sensing of Environment* 229:114–132. <https://doi.org/10.1016/j.rse.2019.04.025>.
- Liu, Chong, Qi Zhang, Shiqi Tao, Jiaguo Qi, Mingjun Ding, Qihui Guan, Bingfang Wu, et al. 2020. "A New Framework to Map Fine Resolution Cropping Intensity across the Globe: Algorithm, Validation, and Implication." *Remote Sensing of Environment* 251:112095. <https://doi.org/10.1016/j.rse.2020.112095>.
- Mahtta, Richa, Anjali Mahendra, and Karen C. Seto. 2019. "Building up or Spreading out? Typologies of Urban Growth across 478 Cities of 1 Million+." *Environmental Research Letters* 14 (12): 124077. <https://doi.org/10.1088/1748-9326/ab59bf>.
- Manupati, Vijaya Kumar, M. Ramkumar, and Digjoy Samanta. 2018. "A Multi-criteria Decision Making Approach for the Urban Renewal in Southern India." *Sustainable Cities and Society* 42:471–481. <https://doi.org/10.1016/j.scs.2018.08.011>.
- Nachmany, Harel, and Ravit Hananel. 2023. "The Urban Renewal Matrix." *Land Use Policy* 131:106744. <https://doi.org/10.1016/j.landusepol.2023.106744>.
- Ni, Hao, Le Yu, and Peng Gong. 2024. "Weakly Supervised Mapping of old and Renewed Urban Areas in China during the Recent two Decades." *International Journal of Applied Earth Observation and Geoinformation* 134:104125. <https://doi.org/10.1016/j.jag.2024.104125>.
- Ni, Hao, Le Yu, Peng Gong, Xuecao Li, and Jiyao Zhao. 2023. "Urban Renewal Mapping: A Case Study in Beijing from 2000 to 2020." *Journal of Remote Sensing* 3:0072. <https://doi.org/10.34133/remotesensing.0072>.
- Olofsson, Pontus, Giles M. Foody, Martin Herold, Stephen V. Stehman, Curtis E. Woodcock, and Michael A. Wulder. 2014. "Good Practices for Estimating Area and Assessing Accuracy of Land Change." *Remote Sensing of Environment* 148:42–57. <https://doi.org/10.1016/j.rse.2014.02.015>.
- Pasquarella, Valerie J., Paulo Arévalo, Kelsee H. Bratley, Eric L. Bullock, Noel Gorelick, Zhiqiang Yang, and Robert E. Kennedy. 2022. "Demystifying LandTrendr and CCDC Temporal Segmentation." *International Journal of Applied Earth Observation and Geoinformation* 110:102806. <https://doi.org/10.1016/j.jag.2022.102806>.
- Potapov, Peter, Matthew C. Hansen, Indrani Kommareddy, Anil Kommareddy, Svetlana Turubanova, Amy Pickens, Bernard Adusei, Alexandra Tyukavina, and Qing Ying. 2020. "Landsat Analysis Ready Data for Global Land Cover and Land Cover Change Mapping." *Remote Sensing* 12 (3): 426. <https://doi.org/10.3390/rs12030426>.
- Qiao, Zhi, Luo Liu, Yuanwei Qin, Xinliang Xu, Binwu Wang, and Zhenjie Liu. 2020. "The Impact of Urban Renewal on Land Surface Temperature Changes: A Case Study in the Main City of Guangzhou, China." *Remote Sensing* 12 (5): 794. <https://doi.org/10.3390/rs12050794>.
- Ratti, Carlo, Nick Baker, and Koen Steemers. 2005. "Energy Consumption and Urban Texture." *Energy and Buildings* 37 (7): 762–776. <https://doi.org/10.1016/j.enbuild.2004.10.010>.
- Reba, Meredith, and Karen C. Seto. 2020. "A Systematic Review and Assessment of Algorithms to Detect, Characterize, and Monitor Urban Land Change." *Remote Sensing of Environment* 242:111739. <https://doi.org/10.1016/j.rse.2020.111739>.
- Ren, Xuefei. 2011. "Olympic Beijing: Reflections on Urban Space and Global Connectivity." In *In the Beijing Olympics: Promoting China: Soft and Hard Power in Global Politics*, edited by Kevin Caffrey, 1011–1039. London: Taylor & Francis Group.

- Seto, Karen C., Burak Güneralp, and Lucy R. Hutya. 2012. "Global Forecasts of Urban Expansion to 2030 and Direct Impacts on Biodiversity and Carbon Pools." *Proceedings of the National Academy of Sciences* 109 (40): 16083–16088. <https://doi.org/10.1073/pnas.1211658109>.
- Solecki, William, Karen C. Seto, and Peter J. Marcotullio. 2013. "It's Time for an Urbanization Science." *Environment: Science and Policy for Sustainable Development* 55 (1): 12–17. <https://doi.org/10.1080/00139157.2013.748387>.
- Song, Xiao-Peng, Joseph O. Sexton, Chengquan Huang, Saurabh Channan, and John R. Townshend. 2016. "Characterizing the Magnitude, Timing and Duration of Urban Growth from Time Series of Landsat-Based Estimates of Impervious Cover." *Remote Sensing of Environment* 175:1–13. <https://doi.org/10.1016/j.rse.2015.12.027>.
- Stehman, Stephen V., and Giles M. Foody. 2019. "Key Issues in Rigorous Accuracy Assessment of Land Cover Products." *Remote Sensing of Environment* 231:111199. <https://doi.org/10.1016/j.rse.2019.05.018>.
- Tu, Ying, Bin Chen, Jun Yang, and Bing Xu. 2023. "Olympic Effects on Reshaping Urban Greenspace of Host Cities." *Landscape and Urban Planning* 230:104615. <https://doi.org/10.1016/j.landurbplan.2022.104615>.
- UN. 2017. "2018 Revision of World Urbanization Prospects." <https://population.un.org/wup/>.
- Verbesselt, Jan, Achim Zeileis, and Martin Herold. 2012. "Near Real-Time Disturbance Detection Using Satellite Image Time Series." *Remote Sensing of Environment* 123:98–108. <https://doi.org/10.1016/j.rse.2012.02.022>.
- Wang, Yixuan, Xuecao Li, Peiyi Yin, Guojiang Yu, Wenting Cao, Jinxiu Liu, Lin Pei, et al. 2023. "Characterizing Annual Dynamics of Urban Form at the Horizontal and Vertical Dimensions Using Long-Term Landsat Time Series Data." *ISPRS Journal of Photogrammetry and Remote Sensing* 203:199–210. <https://doi.org/10.1016/j.isprsjprs.2023.07.025>.
- Wang, Jonathan A., Damien Sulla-Menashe, Curtis E. Woodcock, Oliver Sonnentag, Ralph F. Keeling, and Mark A. Friedl. 2020. "Extensive Land Cover Change across Arctic-Boreal Northwestern North America from Disturbance and Climate Forcing." *Global Change Biology* 26 (2): 807–822. <https://doi.org/10.1111/gcb.14804>.
- Wulder, Michael A., David P. Roy, Volker C. Radeloff, Thomas R. Loveland, Martha C. Anderson, David M. Johnson, Sean Healey, et al. 2022. "Fifty Years of Landsat Science and Impacts." *Remote Sensing of Environment* 280: 113195. <https://doi.org/10.1016/j.rse.2022.113195>.
- Xian, G. Z., K. Smith, D. Wellington, J. Horton, Q. Zhou, C. Li, R. Auch, J. F. Brown, Z. Zhu, and R. R. Reker. 2022. "Implementation of the CCDC Algorithm to Produce the LCMAP Collection 1.0 Annual Land Surface Change Product." *Earth System Science Data* 14 (1): 143–162. <https://doi.org/10.5194/essd-14-143-2022>.
- Xiong, Shuping, Xiuyuan Zhang, Yichen Lei, Ge Tan, Haoyu Wang, and Shihong Du. 2024. "Time-series China Urban Land Use Mapping (2016–2022): An Approach for Achieving Spatial-Consistency and Semantic-Transition Rationality in Temporal Domain." *Remote Sensing of Environment* 312:114344. <https://doi.org/10.1016/j.rse.2024.114344>.
- Xu, Hanqiu. 2006. "Modification of Normalised Difference Water Index (NDWI) to Enhance Open Water Features in Remotely Sensed Imagery." *International Journal of Remote Sensing* 27 (14): 3025–3033. <https://doi.org/10.1080/01431160600589179>.
- Xu, Hanzeyu, Shuhua Qi, Xiao Li, Chen Gao, Yuchun Wei, and Chong Liu. 2021. "Monitoring Three-Decade Dynamics of Citrus Planting in Southeastern China Using Dense Landsat Records." *International Journal of Applied Earth Observation and Geoinformation* 103 (2021): 102518. <https://doi.org/10.1016/j.jag.2021.102518>.
- Xu, Panpan, Nandin-Erdene Tsendbazar, Martin Herold, Sytze de Bruin, Myke Koopmans, Tanya Birch, Sarah Carter, et al. 2024. "Comparative Validation of Recent 10 m-Resolution Global Land Cover Maps." *Remote Sensing of Environment* 311:114316. <https://doi.org/10.1016/j.rse.2024.114316>.
- Ye, Su, Zhe Zhu, and Guofeng Cao. 2023. "Object-based Continuous Monitoring of Land Disturbances from Dense Landsat Time Series." *Remote Sensing of Environment* 287:113462. <https://doi.org/10.1016/j.rse.2023.113462>.
- Yue, Wenze, X. U. Jianhua, Jiawei Wu, and Lihua Xu. 2006. "Remote Sensing of Spatial Patterns of Urban Renewal Using Linear Spectral Mixture Analysis: A Case of Central Urban Area of

- Shanghai (1997–2000).” *Chinese Science Bulletin* 51 (8): 977–986. <https://doi.org/10.1007/s11434-006-0977-8>.
- Zanaga, D., R. Van De Kerchove, W. De Keersmaecker, N. Souverijns, C. Brockmann, R. Quast, J. Wevers, et al. 2021. “ESA WorldCover 10 m 2020 v100.”
- Zha, Y., J. Gao, and S. Ni. 2003. “Use of Normalized Difference Built-up Index in Automatically Mapping Urban Areas from TM Imagery.” *International Journal of Remote Sensing* 24 (3): 583–594. <https://doi.org/10.1080/01431160304987>.
- Zhang, Xiaoxin, Martin Brandt, Xiaoye Tong, Xiaowei Tong, Wenmin Zhang, and Rasmus Fensholt. 2024. “Urban Core Greening Balances Browning in Urban Expansion Areas in China during Recent Decades.” *Journal of Remote Sensing* 4:0112. <https://doi.org/10.34133/remotesensing.0112>.
- Zhang, Chaoqun, Ziyue Chen, Lei Luo, Qiqi Zhu, Yuheng Fu, Bingbo Gao, Jianqiang Hu, et al. 2024. “Mapping Urban Construction Sites in China through Geospatial Data Fusion: Methods and Applications.” *Remote Sensing of Environment* 315:114441. <https://doi.org/10.1016/j.rse.2024.114441>.
- Zhang, Fan, Lun Wu, Di Zhu, and Yu Liu. 2019. “Social Sensing from Street-Level Imagery: A Case Study in Learning Spatio-Temporal Urban Mobility Patterns.” *ISPRS Journal of Photogrammetry and Remote Sensing* 153:48–58. <https://doi.org/10.1016/j.isprsjprs.2019.04.017>.
- Zhang, Lei, Lin Yang, Constantin M. Zohner, Thomas W. Crowther, Manchun Li, Feixue Shen, Mao Guo, Jun Qin, Ling Yao, and Chenghu Zhou. 2022. “Direct and Indirect Impacts of Urbanization on Vegetation Growth across the World’s Cities.” *Science Advances* 8 (27): eabo0095. <https://doi.org/10.1126/sciadv.abo0095>.
- Zhang, Yuanzhi, Hongsheng Zhang, and Hui Lin. 2014. “Improving the Impervious Surface Estimation with Combined use of Optical and SAR Remote Sensing Images.” *Remote Sensing of Environment* 141:155–167. <https://doi.org/10.1016/j.rse.2013.10.028>.
- Zhang, Wei, Xinxin Zhang, and Guangdong Wu. 2021. “The Network Governance of Urban Renewal: A Comparative Analysis of two Cities in China.” *Land Use Policy* 106:105448. <https://doi.org/10.1016/j.landusepol.2021.105448>.
- Zhang, X., T. Zhao, H. Xu, W. Liu, J. Wang, X. Chen, and L. Liu. 2024. “GLC_FCS30D: The First Global 30M Land-Cover Dynamics Monitoring Product with a Fine Classification System for the Period from 1985 to 2022 Generated Using Dense-Time-Series Landsat Imagery and the Continuous Change-Detection Method.” *Earth System Science Data* 16 (3): 1353–1381. <https://doi.org/10.5194/essd-16-1353-2024>.
- Zhao, Jiyao, Guangzhao Chen, Le Yu, Chao Ren, Jing Xie, Lamuel Chung, Hao Ni, and Peng Gong. 2023. “Mapping Urban Morphology Changes in the Last two Decades Based on Local Climate Zone Scheme: A Case Study of Three Major Urban Agglomerations in China.” *Urban Climate* 47:101391. <https://doi.org/10.1016/j.uclim.2022.101391>.
- Zhao, Xin, Yi Hu, Nan Xia, ManChun Li, Dengshuai Chen, and Yunyun Xu. 2024. “Urban Regeneration and SDGs Assessment Based on Multi-source Data: Practical Experience from Shenzhen, China.” *Ecological Indicators* 165:112138. <https://doi.org/10.1016/j.ecolind.2024.112138>.
- Zhao, Xin, Nan Xia, and ManChun Li. 2023. “Dynamic Monitoring of Urban Renewal Based on Multi-source Remote Sensing and POI Data: A Case Study of Shenzhen from 2012 to 2020.” *International Journal of Applied Earth Observation and Geoinformation* 125:103586. <https://doi.org/10.1016/j.jag.2023.103586>.
- Zheng, Helen Wei, Geoffrey Qiping Shen, and Hao Wang. 2014. “A Review of Recent Studies on Sustainable Urban Renewal.” *Habitat International* 41:272–279. <https://doi.org/10.1016/j.habitatint.2013.08.006>.
- Zhou, Yuyu, Xuecao Li, Wei Chen, Lin Meng, Qiusheng Wu, Peng Gong, and Karen C. Seto. 2022. “Satellite Mapping of Urban Built-up Heights Reveals Extreme Infrastructure Gaps and Inequalities in the Global South.” *Proceedings of the National Academy of Sciences* 119 (46): e2214813119. <https://doi.org/10.1073/pnas.2214813119>.
- Zhu, Zhe, Alisa L. Gallant, Curtis E. Woodcock, Bruce Pengra, Pontus Olofsson, Thomas R. Loveland, Suming Jin, Devendra Dahal, Limin Yang, and Roger F. Auch. 2016. “Optimizing

- Selection of Training and Auxiliary Data for Operational Land Cover Classification for the LCMAP Initiative.” *ISPRS Journal of Photogrammetry and Remote Sensing* 122:206–221. <https://doi.org/10.1016/j.isprsjprs.2016.11.004>.
- Zhu, Zhe, Curtis E. Woodcock, Christopher Holden, and Zhiqiang Yang. 2015. “Generating Synthetic Landsat Images Based on All Available Landsat Data: Predicting Landsat Surface Reflectance at Any Given Time.” *Remote Sensing of Environment* 162:67–83. <https://doi.org/10.1016/j.rse.2015.02.009>.
- Zhu, Zhe, Junxue Zhang, Zhiqiang Yang, Amal H. Aljaddani, Warren B. Cohen, Shi Qiu, and Congliang Zhou. 2020. “Continuous Monitoring of Land Disturbance Based on Landsat Time Series.” *Remote Sensing of Environment* 238:111116. <https://doi.org/10.1016/j.rse.2019.03.009>.
- Zhu, Zhe, Yuyu Zhou, Karen C. Seto, Eleanor C. Stokes, Chengbin Deng, Steward T. A. Pickett, and Hannes Taubenböck. 2019. “Understanding an Urbanizing Planet: Strategic Directions for Remote Sensing.” *Remote Sensing of Environment* 228:164–182. <https://doi.org/10.1016/j.rse.2019.04.020>.
- Zhuo, Li, Runjie Huang, Chuyao Liao, Haiyan Tao, and Yunze Zang. 2024. “BATSCCD: A new Change Detection Method for Mapping Building age in Rapidly Changing Urban Areas Using Landsat Time Series Data.” *International Journal of Digital Earth* 17 (1): 2358859. <https://doi.org/10.1080/17538947.2024.2358859>.